HIFI FM Radiometry measurements

Hifi no.: SRON-G/HIFI/TR/2008-001.
Inst.no.: n
Issue: Draft 1.1
Date: :09-04-08
Category: 2.

Prepared by: Bengt Larsson, David Teyssier — Date: 9 April 2008

Checked by: Pieter Dieleman, Michael Olberg — Date: 19 March 2008

Agreed PA: — Date:

Authorised by: — Date:

Distribution:

HIFI ICC

ESADocument Change Record

Date	Issue/Revision	Change
20/03/08	Draft 1.0	First draft.
09/04/08	Issue 1.1	Included comments from M. Olberg and P. Dieleman Added HRS data Added inputs from T. Peacocke and W. Jellema on expectation from optical models.

Table of contents

1. Introduction 2

2. References 2

a. Applicable Documents 2

b. Reference Documents 2

3. Test set-up and measurement principle 3

4. Overview of the measurements..... 5

5. Data processing and data repository..... 5

6. Receiver noise temperature and source coupling determination 6

7. Source coupling as a calibration product 18

Introduction

This document describes the test campaigns and associated results of the pre-launch calibration activity dedicated to the radiometric properties of the HIFI Flight Model. It provides a detailed overview of the measurement objectives, the strategy implemented, and of the data analysis and its inputs into the calibration equation.

ESAC 7/26/06 2:01 PM
Formatted: Bullets and Numbering

References

ESAC 7/26/06 2:01 PM
Formatted: Bullets and Numbering

a. Applicable Documents

AD1	SRON-G/HIFI/PL/1999-001	AIV plan for HIFI	Issue 1.0
AD2	LRM-ENS/HIFI/PL/2000-001	Calibration Plan for HIFI	Issue 1
AD3	SRON-G/HIFI/PL/2001-001	Detailed test plan of HIFI Instrument Tests	Draft 0.3
AD4	ICC/2001-005	HIFI calibration use cases	Draft 0.3

b. Reference Documents

RD1	SRON-U/HIFI/SP/2001-009	Test-equipment interface URD	Issue 1.1
RD2	Alma memo 442	The intensity calibration for HIFI	Issue 1.0
RD3	SRON-G/HIFI/TN/2004-xxx	Absolute Hot BB for HIFI AIV/ILT	Issue 0.1
RD4	NDW – SRON - 2004-10-05	Reflectometer test analysis	Issue 1.0
RD5	SRON-G/HIFI/ILT/2007-01200	HIFI System stability	Issue 1.0

c. Information repository

The radiometry working group has a wiki page gathering all the relevant information and some details that will not be repeated in this report. Please visit:

http://www.sron.rug.nl/~wikiman/wikis/HifiIlt/RadiometryTeamPages

d. Acronyms

AHBB	Absolute Hot Black Body
ACBB	Absolute Cold Black Body (“the shutter”)
COA	Common Optic Assembly
CSA	Common Source Assembly
CBB	Cold Black Body

HBB	Hot Black Body
HK	HouseKeeping

Test set-up and measurement principle

ESAC 7/26/06 2:01 PM
Formatted: Bullets and Numbering

3.1 Objectives

Following AD4, the goal of the radiometry activity is twofold:

- Measurement of the instrument sensitivity, as given by the receiver noise temperature.
- Measurement of the mixer beam coupling onto the internal calibration sources (hot and cold sources, hereafter HBB and CBB respectively)

Each of the above quantities needs to be surveyed over the full HIFI frequency range, with a granularity of at least 4 GHz.

3.2 Measurement principles

Both quantities above can be measured together, following a 4-step measurement approach.

- The assessment of the mixer beam coupling to the sources can be done by calibrating the temperature measured against the internal black bodies against absolute photometric calibrators, which we will call AHBB and ACBB (see next section)
- Once the coupling are known, the system noise temperature can be derived from the so-called Y-factor, which is the ratio between total power mixer counts obtained towards the HBB and the CBB respectively.

The measurement sequence consists of the following:

- Total-power measurement towards the AHBB: V_{AHBB}
- Total-power measurement towards the ACBB: V_{ACBB}
- Total-power measurement towards the HBB: V_{HBB}
- Total-power measurement towards the CBB: V_{CBB}

Because gain drift can be significant in some LO bands, the total-power scheme listed above can be replaced by a slow-chop alternative, all main line-of-sight being chopped against the CBB. In this option, the coupling towards the CBB cannot be obtained as the problem is degenerated and its value needs to be estimated beforehand.

3.3 The external black bodies

A detailed description of the design and manufacturing of the AHBB can be found in RD3. This test equipment can be directly coupled on top of the FM test cryostat, offering a beam filled absolute photometric reference for any aperture on the M3 folding mirror. The reflection coefficient for this black body has been measured to be of the order of -50 dB (RD4). No coherent reflection (standing wave) related to the top plate of the cavity was observed in the measurements.

The physical temperature to be assigned to the AHBB depends on the cooling time. It was shown that, once totally stabilised, the temperature difference between the top of the cavity and the bottom collar is less than 1K. The absolute temperature is then of the order of 95K Given the high fraction of the beam coupled to the top plate of the cavity, the physical temperature of the black body can then be taken from the temperature sensor located on this plate. When the delta is larger, corrections (lower effective temperature) have to be applied.

To act as the ACBB, we have used the so-called “shutter” or cold-flap, located right on top of the M3 mirror in the test cryostat. This is a tilted SiC coated plate offering a complete termination for all apertures on M3. Its temperature is measured by a dedicated temperature sensor, and is of the order of 10K. Figure 1 sketches the two black bodies.

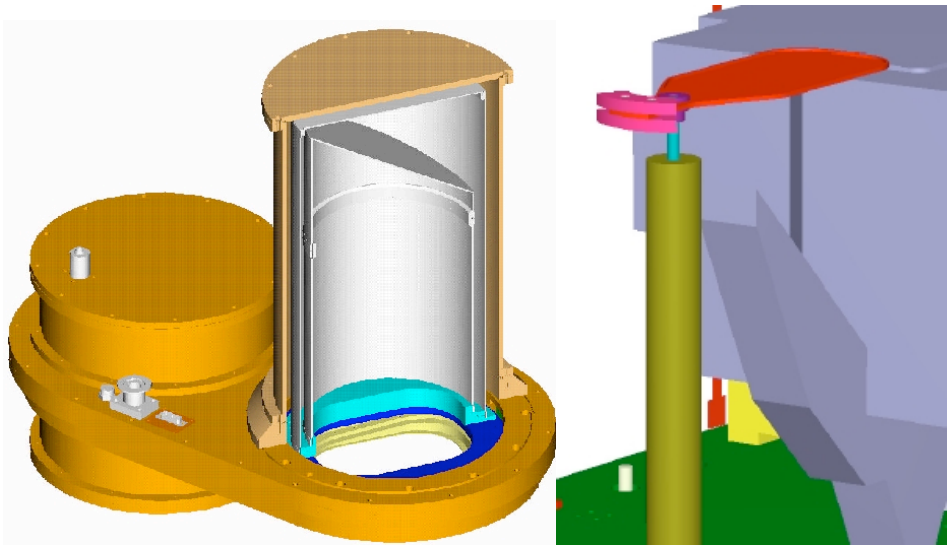

Fig. 1: Left: AHBB cut, showing the inner cavity profile, and the various shields as well as the LN2 vessel. Right: ACBB (shutter) located above the M3 mirror

3.4 Source coupling in the calibration equation, and impact

Following RD2, the calibrated data will be obtained following:

$$J_{source} - J_{OFF} = \frac{1}{G_{ssb}\eta_l + \omega_{ssb}} \frac{\eta_{hot} + \eta_{cold} - 1}{\eta_{sf}} \times [...]$$

The contribution to the calibration error budget is:

- 1% error on η_{hot} corresponds to 1% error on the absolute calibration at any frequency

- 1% on η_{cold} corresponds to 0.2% error in the absolute calibration at 500GHz, and 0.5% at 1900 GHz

Overview of the measurements

ESAC 7/26/06 2:01 PM
Formatted: Bullets and Numbering

Radiometry measurements have been performed over 3 dedicated campaigns: February 2007, April 2007 and June 2007. In between these campaigns, several instrument configuration changes have occurred, the main one being the insertion of attenuators between in the LOU and the FPU after the April campaign. Therefore, the full set of data has been unequally affected by the caveats of the test environment.

The following table summarized the configuration applying to the data acquired. Further details can be found on the wiki pages.

Test campaign	February 07	April 07	June 07
Bands covered	1,2,4,5,6	3,7	2b, 4, 6, 7
Sampling	4 GHz	4 GHz	4 GHz
Database	fm_ilt_3	fm_ilt_4	fm_ilt_5
Obsid's	268462205 to 268463331	268468554 to 268469181	268516923 to 268517635
H/W config	No LOU attenuators	No LOU attenuators	LOU attenuators
Remarks	Band 6 data done in fast-chop.	268468554 to 268468711 are corrupted	Temperature of AHBB not settled All measurements in fast-chop

Tale 1: summary table for the radiometry measurement campaigns

Beside these campaign, a dedicate receiver noise temperature survey has been performed with a granularity of 1 GHz. This survey was conducted between 17 and 19 May 2007. It concerns obsid's in the range 268485136 to 268496226, and is stored in fm_ilt_5.

Data processing and data repository

ESAC 7/26/06 2:01 PM
Formatted: Bullets and Numbering

Raw data from the database have been processed using the standard pipeline. Although data have been obtained simultaneously by both backends (in both polarizations), this report only concentrates on the WBS data. Frequency scales have been calibrated in the pipeline using the COMB measurements.

A data pool will be created to store all pipelined data, as well as the reduced spectra providing the receiver temperature and source coupling spectra (see algorithms thereafter).

Receiver noise temperature and source coupling determination

6.1 Definition of the receiver noise temperature

We define the *Y*-factor as follows:

$$Y = \frac{V_{HBB}}{V_{CBB}}$$

If J_{Hot} and J_{Cold} are the Rayleigh-Jeans temperatures of the respective internal loads at the frequency of interest, the receiver noise temperature is given by:

$$T_{rec} = \frac{J_{Hot} - YJ_{Cold}}{Y - 1}$$

Consequently, the system noise temperature will be given by

$$T_{sys} = J_{bg,eff} + \frac{1-\eta_l}{\eta_l} \times J_{T,eff} + \frac{T_{rec}}{\eta_l}$$

where η_l is the forwards efficiency, $T_{bg,eff}$ the cosmic background temperature, and $J_{T,eff}$ the effective telescope temperature.

6.2 Definition of the source coupling

With the quantity introduced in 3.2, we form the following differenced signals:

$$\Delta V_1 = V_{AHBB} - V_{ACBB} = \gamma[\eta_{AHBB} J_{eff,AHBB} - \eta_{ACBB} J_{eff,ACBB}]$$

where γ is the instrumental gain, $J_{eff} = G_s J_s + (1-G_s)J_i$ is the effective radiation temperature seen in both image and signal side-bands, and η_{AHBB} and η_{ACBB} are the global transmission along the respective corresponding optical paths. All Rayleigh-Jeans temperatures can be deduced from the known physical temperatures of the loads (including emissivity correction).

and

$$\Delta V_2 = V_{HBB} - V_{ACBB} = \gamma[\eta_{hot}\eta_{HBB} J_{eff,HBB} - \eta_{ACBB} J_{eff,ACBB}]$$

where η_{HBB} is the transmission along the HBB optical path and η_{hot} represents the radiative coupling to the physical temperature featured by the HBB (and expressed here by $J_{eff,HBB}$).

The effective HBB radiation temperature can be computed as follows:

$$\eta_{hot} J_{eff,HBB} = \frac{\Delta V_1}{\Delta V_2} \times \frac{\eta_{AHBB} J_{eff,AHBB} - \eta_{ACBB} J_{eff,ACBB}}{\eta_{HBB}} + \frac{\eta_{ACBB}}{\eta_{HBB}} J_{eff,ACBB}$$

and if required, isolate η_{hot}.

Similarly, for the CBB we can form.

$$\Delta V_2 = V_{CBB} - V_{ACBB} = \gamma[\eta_{cold}\eta_{CBB} J_{eff,CBB} - \eta_{ACBB} J_{eff,ACBB}]$$

and

$$\eta_{cold} J_{eff,CBB} = \frac{\Delta V_1}{\Delta V_2} \times \frac{\eta_{AHBB} J_{eff,AHBB} - \eta_{ACBB} J_{eff,ACBB}}{\eta_{CBB}} + \frac{\eta_{ACBB}}{\eta_{CBB}} J_{eff,ACBB}$$

If required, isolate η_{cold}.

Note: In order to derive the effective HBB temperature, one needs to make some assumptions on the optical transmissions involved in the equation. We will assume $\eta_{CBB} \approx \eta_{HBB} \approx \eta_{ACBB} \approx \eta_{AHBB}$, although there might be extra transmission losses induced by the polyethylene window isolating the AHBB from the cryostat. We will not consider them significant.

6.3 Hardware and environment limitations

6.3.1 Instrument tuning capabilities

Because of the high dynamic in the LOU output power, not all sky frequencies can be effectively pumped. Indeed, in some LO frequency area, the mixer cannot be pumped to a level providing a decent sensitivity. This ends up as gaps in the coverage.

6.3.2 Instrument stability

Because the source coupling determination makes use of measurements taken at different times, the final result is sensitive to gain drifts. During the HIFI FM campaign, it has been shown that operations of the LOU without attenuators would lead to quite poor Allan time, resulting in relatively strong drifts and poor baselines (see RD5).

These potential baseline distortions are mostly present in bands 2b, 4a, 4b, and all HEB bands. They are clearly affecting the data of the February and April campaigns. In June, measurements performed with the attenuators in place showed an improvement in the SIS bands, but HEB bands are still suffering from drifts.

Fig. 2 and 3 illustrate such effects in bands 4a and 7a.

On top of this, it has been noted that the rotation of metal pieces inside the FM test cryostat could create some feedback at the IF level. In practice, when moving the chopper (M6) or the shutter, the IF response is modified and the differences in the measurements show up as strong scatter in the receiver noise and source coupling spectra, especially at the band edges. In order to mitigate this we have tried to adapt the measurement scheme so that total power spectra against the internal loads would be obtained for both the open and the closed shutter. However, by essence, the calibration of the internal source effective temperature needs both the measurements against the AHBB and the shutter, implying a rotation of that latter. Fig. 4 illustrates such effect in band 1b. Finally, spurious signals can show up at sporadic places in the IF spectrum. Fig. 4 also shows one of these spikes (CCD1 of the WBS).

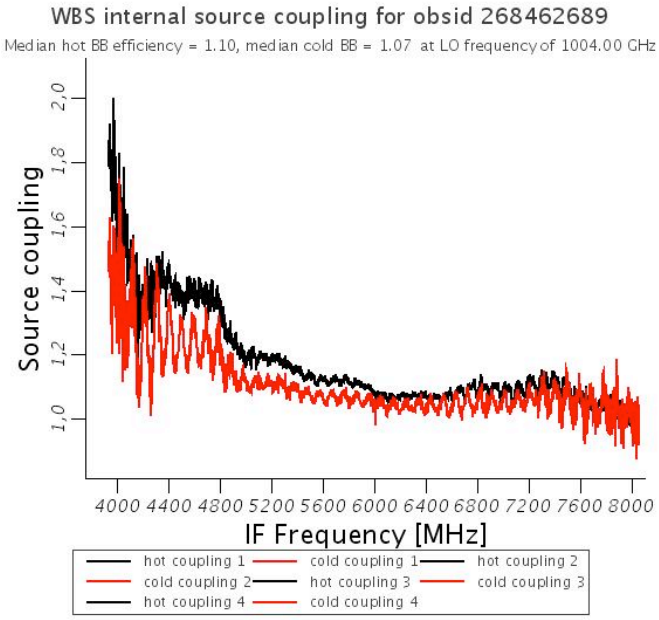

Fig 2: illustration of baseline distortion in band 4a (1004 GHz). It shows up here as baseline ripple (period ~ 170 MHz) and strong excess noise at the band edge.

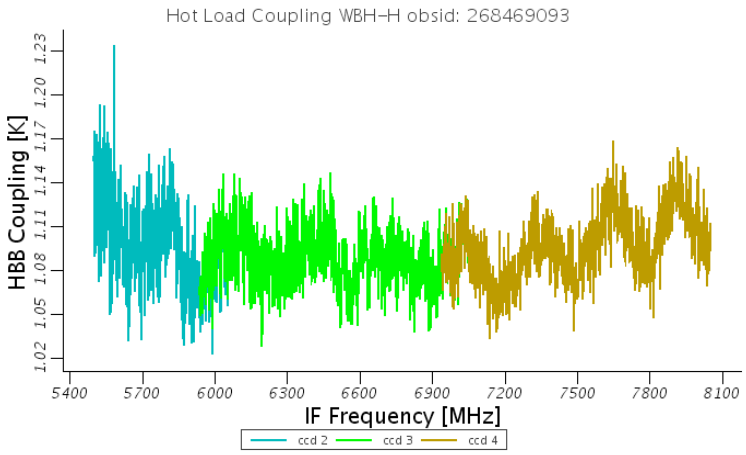

Fig.3: illustration of standing waves affecting the source coupling spectra in HEB bands. Example given for band 7a at 1824 GHz.

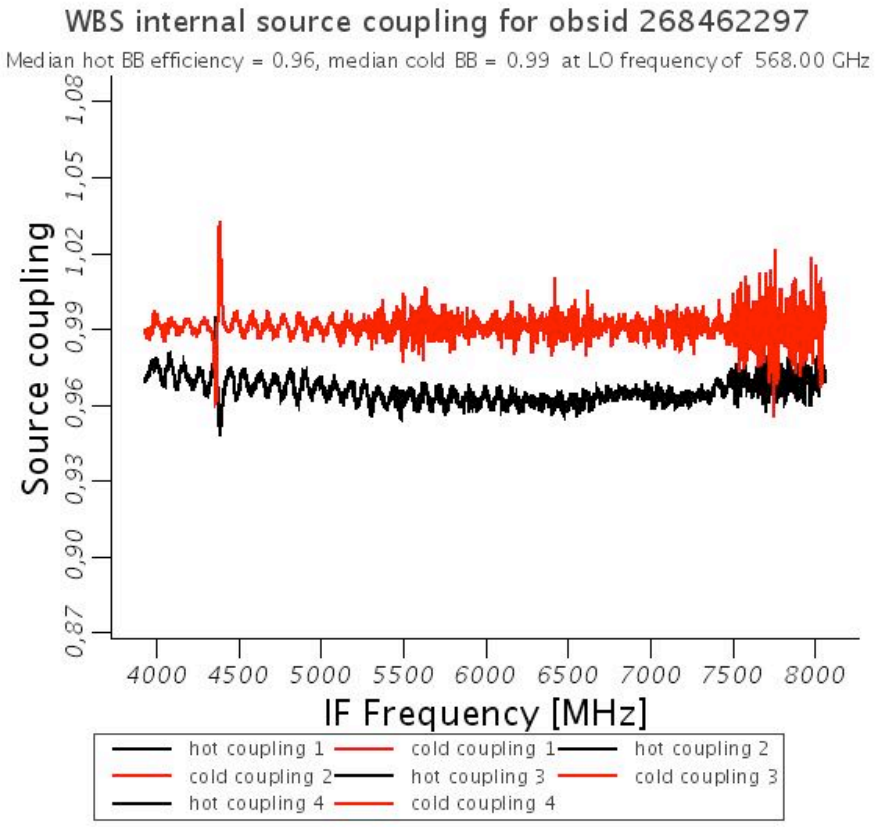

Fig 4: illustration of baseline distortion in band 1b (568 GHz), as well as IF feedback effect (esp. higher end of the IF). It shows again the baseline ripple of period ~ 170 MHz, and spurious signal at IF ~ 4.4 GHz.

6.4 Receiver noise temperature results

6.4.1 Radiometry measurements

February-April 07 data

The following plot compiles all receiver noise measurements for the campaigns of February and April 07. For each LO frequency, the receiver noise is taken as the median of the full IF spectrum. This allows to smooth out standing wave and potential IF feedback effects. Note the poor results in bands 6a and 6b in the V-mixer. This is due to the incapability of correctly

pumping this mixer with the strong LO output power imbalance between the two polarizations.

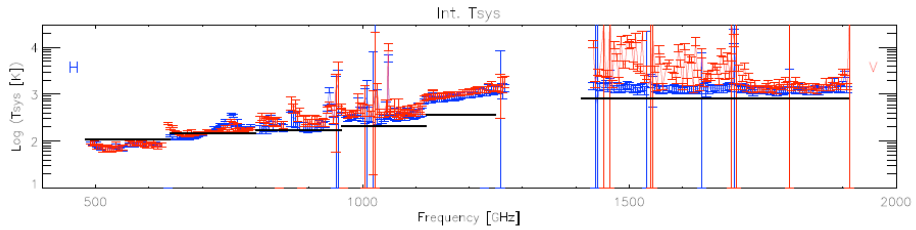

Fig 5: Overview of the receiver noise temperature (sampling 4 GHz) as measured during the February and April campaigns (Blue: H-polarization, Red: V-polarization). Black lines indicate the respective mixer band coverages. Error bars correspond to the 1 sigma rms on the noise spectra.

The following plot shows the same receiver noise result, but this time represents the full IF spectra for each measurement. It illustrates the strong scatter in many of the measurements, as well as the instable areas, e.g. in 4a.

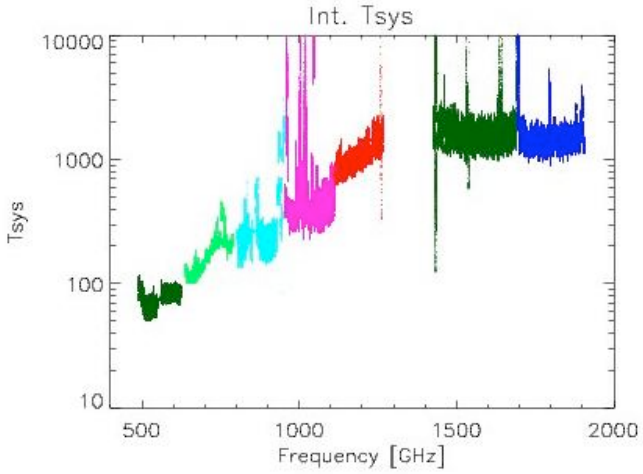

Fig 6: concatenation of receiver noise temperature IF spectra over the spanned LO range.

June 07 data

Same as above, but this time, data from June 07 are merged and, whenever justified, substitute the poor results of the previous campaigns. Note the improvement in mixer V for the band 6. This is due to an improved imbalance between the two polarization when

introducing the LOU attenuator filters. On the other hand, the new filters have created new gaps, as e.g. at the upper end of band 2b.

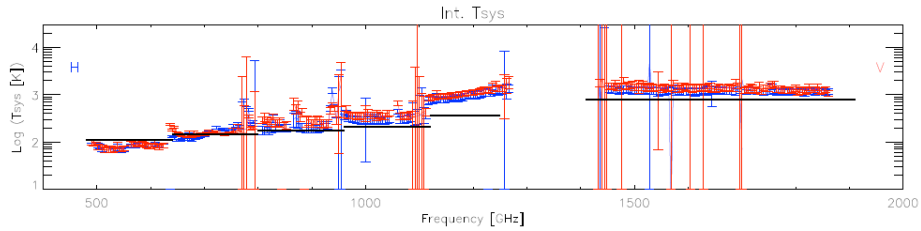

Fig 7: Same as Fig 5 with the June 07 data included

6.4.2 High granularity measurements

These data were collected with the attenuators in place, so they provide the most representative coverage of the HIFI instrument sensitivity. The plots below have been re-binned to provide a smoother appearance. The gaps however have been kept untouched to not be smeared to the rest of the data set.

Further, we show the best noise temperature available for a given LO frequency. Finally, we show the best available noise temperature for a given sky frequency. Both mixers are indicated, as well as the radiometric average of both.

6.5 Source coupling results

6.5.1 Data from February and April 07 campaigns

Fig. 8 gathers all hot and cold source coupling factors. They correspond to the median of the source coupling spectra computed as indicated in section 6.2. Error bars are the rms of those spectra.

The general trend is that of a coupling very close to 1, as is predicted by quasi-optical simulation. Departure from unity can be due to *i)* real optical mis-alignement, *ii)* un-stable measurements leading to non-physical results. The coupling to the cold load is basically unity everywhere. The coupling to the hot load experiences a slow rise in bands 1a and 1b, then settles around unity.

It is interesting to note how the IF feedback effects enhance the apparent error bars in band 5. Also, instabilities in bands 2a, 4a and 4b create a more scattered pattern. Finally, coupling in bands 6 and 7 are totally dominated by large scatters and error bars. As was shown above, measurements of mixer V in band 6 are useless for these measurement campaigns as the mixer could not be correctly tuned.

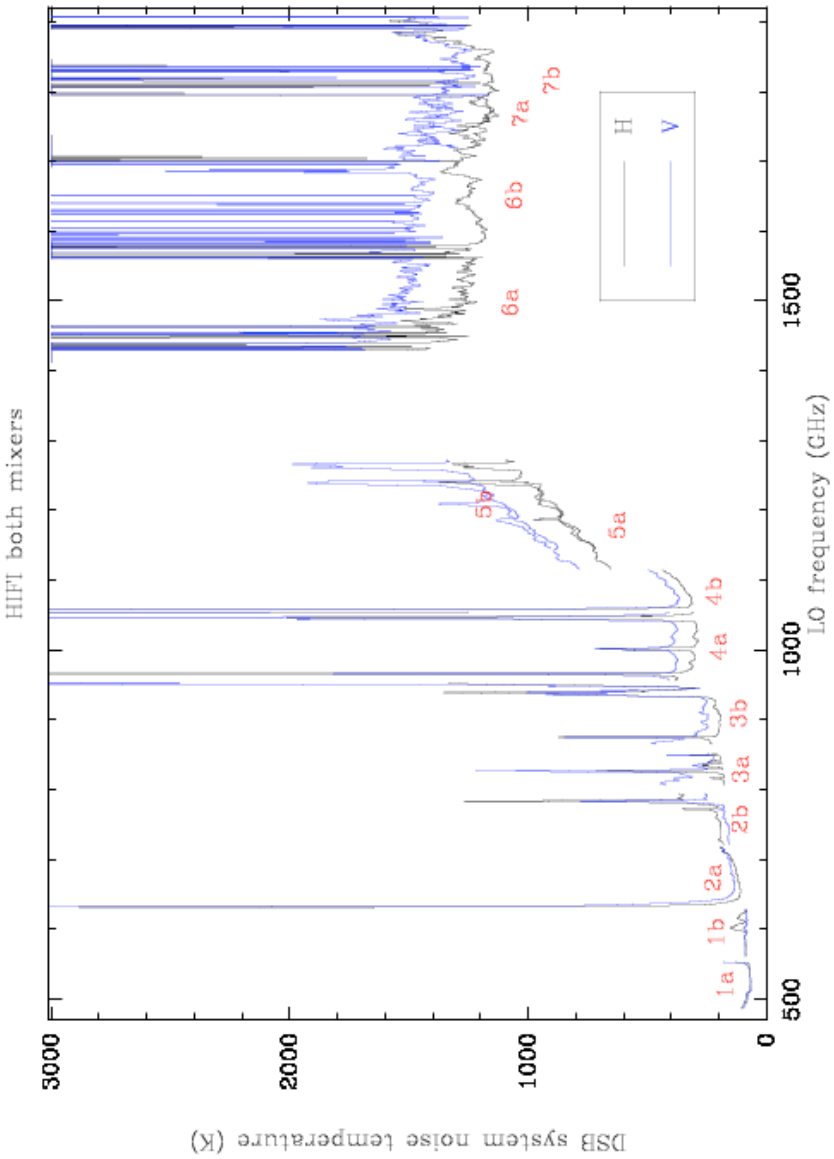
HIFI both mixers
DSB system noise temperature (K)
LO frequency (GHz)
H
V
1a
1b
2a
2b
3a
3b
4a
4b
5a
5b
6a
6b
7a
7b
0
1000
2000
3000
500
1000
1500

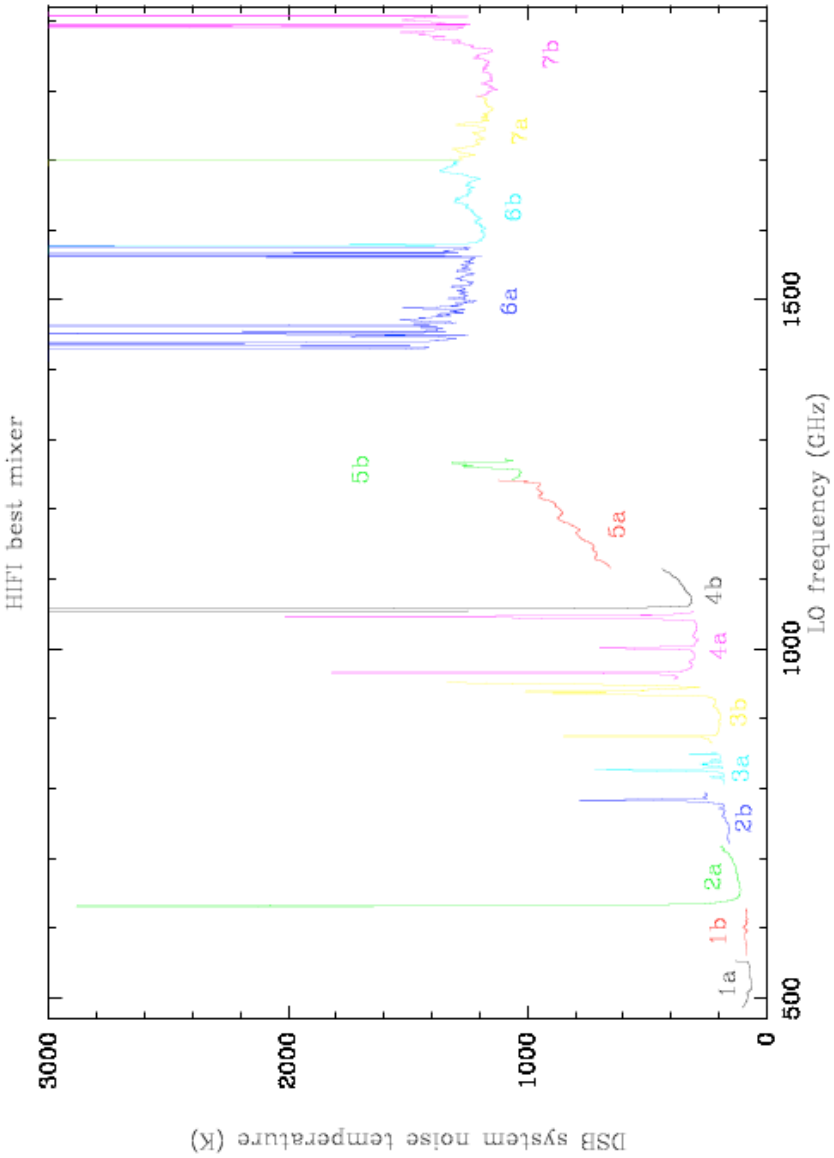
HIFI best mixer
LO frequency (GHz)
DSB system noise temperature (K)
500
1000
1500
0
1000
2000
3000
1a
1b
2a
2b
3a
3b
4a
4b
5a
5b
6a
6b
7a
7b

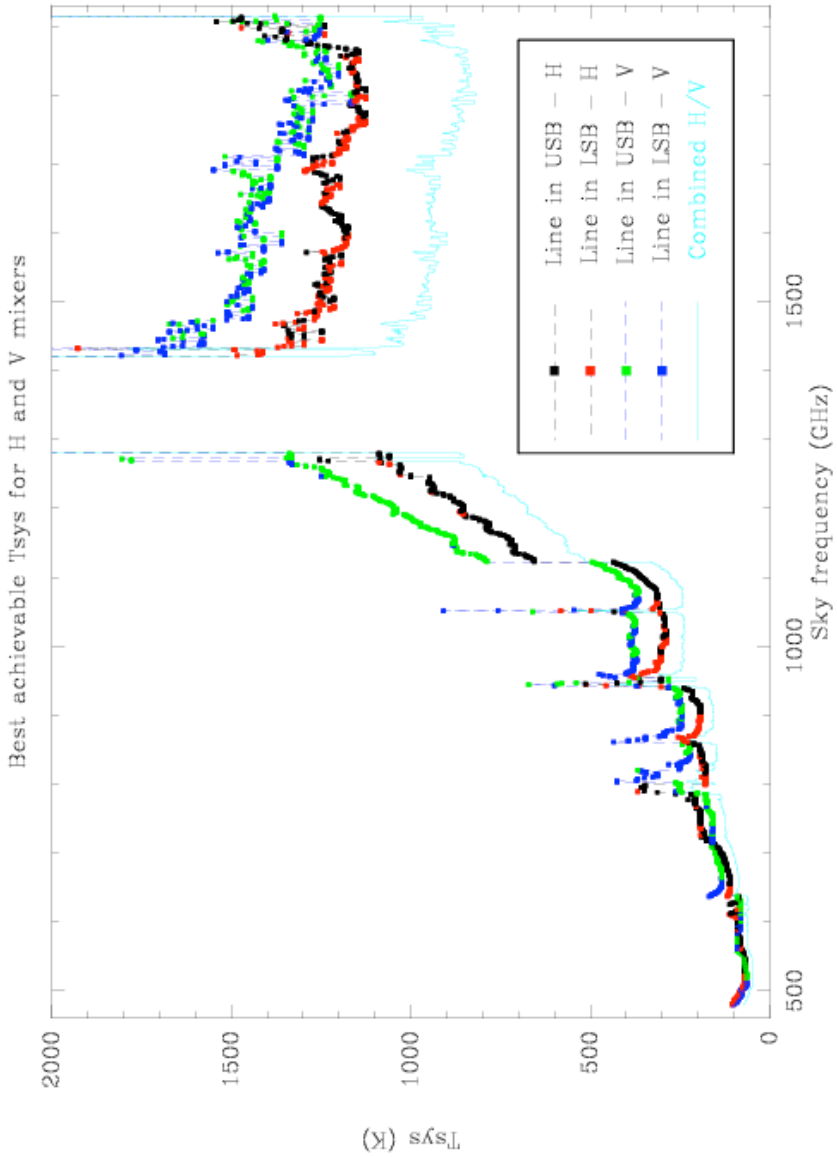
Best achievable Tsys for H and V mixers
Tsys (K)
Sky frequency (GHz)
Line in USB - H
Line in LSB - H
Line in USB - V
Line in LSB - V
Combined H/V
0
500
1000
1500
2000
500
1000
1500

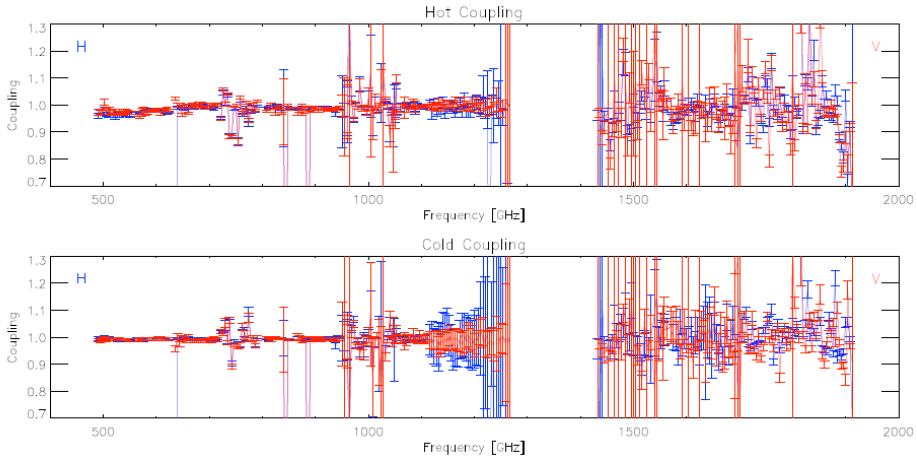

Fig 8: Compilation of hot and cold source coupling for the February and April 2007 campaigns

6.5.2 Data from June 07 campaign

Figure 9 below shows the same results with June 07 measurements replacing those of the previous campaign for bands 2a, 4, 6 and 7.

The first striking thing is a systematic offset appearing in the hot load coupling. At the same time, the strong scatter of the previous campaigns has been much improved, this because of an enhanced stability thanks to the introduction of the attenuator, as well as to the chopped observing scheme, more robust against quick drift. Also, data in mixer V of band 6 are now obtained with a decently pumped mixer. Some scatter remains in the HEB bands though.

To understand why an offset affects the new data, we have inspected the housekeeping (HK) for the external load temperature. It appears that this temperature was decreasing during the whole measurement slot (from 110 to 87 K, in an exponential fashion), meaning that the AHBB cavity was not thermally stabilized. It also means that the physical temperature seen by the mixer was lower than the estimated one, given by the sensor at the top of the cavity. Figure 9 illustrates this decrease for the time slot corresponding to bands 2 and 4 measurements.

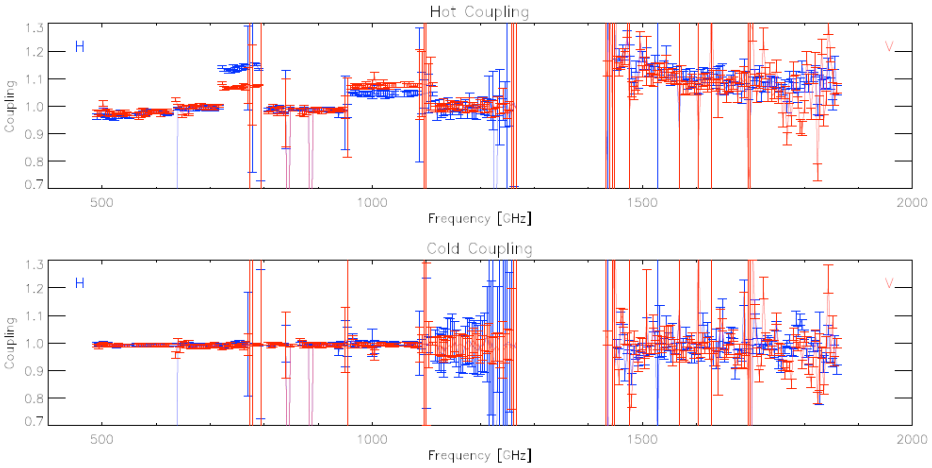

Fig 9: Same as Fig 8 with June 2007 campaign included

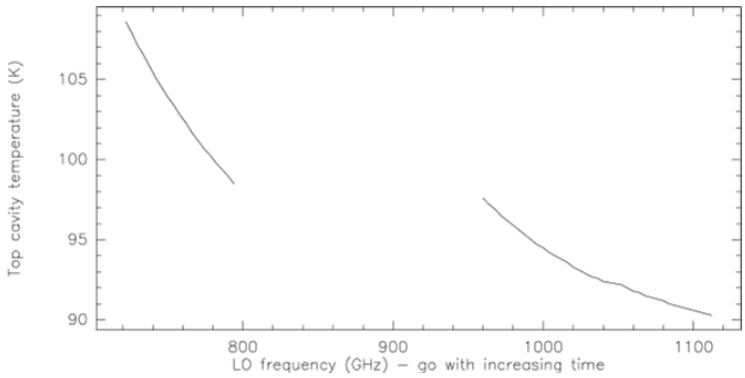

Fig 10: Illustration of the top cavity temperature decrease with time.

We have tried to link the measured temperature at the top of the cavity to an effective temperature seen by the mixer. For this, an important information is the temperature at the bottom of the cavity, which indicates the gradient over the black body height. Unfortunately, it turned out that this temperature sensor was not available during the test, as its connector was needed to monitor another unit. Therefore, we have deduced that there was no accurate way to recover the absolute temperature of the reference black body, making thus un-usable the whole June data-set. It however serves to show the improvement gained due to the new

observing scheme and the use of attenuators, but also shows that even in these improved conditions, data taken with the HEB bands are still affected by gain drifts.

6.5.3 Redundant measurements

In addition to the point presented so far, all measurements have been usually repeated once or twice at all frequencies. This was done in order to check reproducibility of the results. We have found a high level of reproducibility for the coupling efficiencies retrieved from measurements not significantly affected by any of the un-stability effects mentioned here. These additional measurements have not been included in the statistics described in the next section.

Source coupling as a calibration product

7.1 Final source coupling coefficients

In this section, we do a synthesis of all the data compiled in the previous section in the perspective of preparing the final calibration product that should end up in the calibration database.

As shown previously, despite of all precautions taken and the careful design of the test equipments, there remain strong scatters in the final results. The question is whether these should propagate to the pipeline, i.e. whether they should be considered real. Theory indicates very much that most coupling should be at unity, this especially at high frequencies where the mixer beam size is relatively small compared to the load optics. In order to strongly depart from unity, there should be a quite significant mis-alignment inside the FPU, which is not supported by other measurements (e.g. beam measurements). The exception is likely the case of band 1, where the beam is slightly oversized w.r.t. the HBB aperture at the lowest frequencies, and where spill-over can play a role. For this latter, although theory also shows that a perfectly aligned system should end up with a perfect coupling, the trend seen in the data is clearly real. Such an effect could be possible especially in the case of the measured pupil misalignment, tilt and defocus in MSA band 1. However it is not totally clear why a frequency dependence is observed, and running dedicated models accounting for all effects would be too time-consuming. So we have decided to take the measurement data at face-value, and to reflect the trend in the coupling (see below).

In addition, we have decided not to use the data measured for bands 2b and 4a during the February campaign, as we considered that the high level of un-stability made them un-reliable. Instead, we have limited the fit to the respective 2a and 4b data, assuming that the coupling would not differ significantly over the mixer band range. As indicated earlier, we could also not use the June data for these sub-bands, since we have not been able to accurately recover from the offset due to the thermally un-settled external load.

All in all, we have decided to consider one single number per mixer band, and assign to it an error corresponding to the scatter of the measured point in this band. In band 1 though, we have decided to reflect the rising trend of the hot load coupling. For this purpose, we have fitted a slope to the rising trend across the frequency range. The result of these fits is compiled in the following table. The min and max frequencies (given in GHz) indicate the ranges used for the fit – of course the couplings given here should be used for the whole frequency range applying to a mixer band.

Band	Start Freq	Stop Freq	Coupling	Coup. Err.	Slope	Slope err.	Freq0
Cold couplings – WBS-H polarization							
1	494	620	0.991	1.9E-3	0	0	0
2	640	716	0.993	1.7E-3	0	0	0
3	816	942	0.996	1.0E-3	0	0	0
4	1060	1108	0.997	1.3E-3	0	0	0
5	1116	1266	0.987	1.7E-2	0	0	0
6	1432	1692	0.994	3.3E-2	0	0	0
7	1708	1908	0.998	3.5E-2	0	0	0
Hot couplings – WBS-H polarization							
1	498	624	0.969	8.84E-4	1.3E-4	2.01E-5	561
2	640	716	0.993	4.2E-3	0	0	0
3	808	938	0.988	2.6E-3	0	0	0
4	1064	1112	0.996	2.4E-3	0	0	0
5	1116	1258	0.993	1.7E-2	0	0	0
6	1432	1692	0.982	2.0E-2	0	0	0
7	1704	1908	0.970	2.3E-2	0	0	0
Cold couplings – WBS-V polarization							
1	506	620	0.992	1.2E-3	0	0	0
2	660	716	0.988	2.2E-3	0	0	0
3	816	942	0.992	2.2E-3	0	0	0
4	1064	1112	0.994	3.2E-3	0	0	0
5	1116	1266	0.985	9.6E-2	0	0	0
6	1436	1696	0.992	5.2E-2	0	0	0
7	1704	1900	0.985	4.3E-2	0	0	0
Hot couplings – WBS-V polarization							
1	494	624	0.976	9.72E-4	7.9E-5	2.23E-5	559
2	644	716	0.996	7.6E-3	0	0	0
3	812	942	0.987	2.8E-3	0	0	0
4	1064	1112	0.996	4.2E-3	0	0	0
5	1120	1266	0.996	1.0E-2	0	0	0
6	1436	1696	0.984	4.0E-2	0	0	0
7	1708	1908	0.973	2.9E-2	0	0	0

Table 2: Final coupling numbers for each mixer as derived from the WBS

7.2 Expectation from optical models

From a modelling point of view, assuming perfectly aligned COA and CSA optics, the fraction of power in the beam incident on the HBB aperture that makes it to the insides of the HBB blackbody is nearly unity everywhere.

That does however not imply that the total blackbody coupling is unity everywhere. First of all the temperature we assume (based on the sensor) might be slightly different than the effective surface temperature of the SiC foam. Secondly, the emissivity is probably not 100%. Finally, ohmic losses in the mirrors are not taken into account in the optical modelling. On the other hand, we do calibrate relative to an external blackbody and the difference in number of mirrors to external blackbody and HBB is identical. Apart from the two CSA mirrors, whose ohmic losses are expected to be very small, that could give a slight difference between the cold and hot load coupling (since looking at the HBB involves two more mirrors).

Given the fact that the system is not perfectly aligned, and since we do not have accurate misalignment information of each single optical component, there is not much we can model and we in fact have to rely on end-to-end measurements. Even though the optical coupling is expected to be nearly unity, we can't simply assume this to be true and include it in our calibration budget, because of possible misalignments, ohmic losses, frequency dependent emissivity and temperature gradients.

One key issue here is whether or not we should include frequency dependence of the coupling. On a band to band basis experts are inclined to say that we do not expect strong frequency dependence here (apart from band 1, where they agree that the HBB characteristic is most likely real and systematic and probably needs first-order frequency dependence included). If we have strong reasons to believe that the scatter really comes from the calibration measurement method, and we can justify that we do not expect significant frequency dependence (supported by e.g. SiC foam sample level emissivity measurements, mirror level measurement of ohmic losses and optical tolerance analysis + frequency domain analysis), we do have a strong case to take the average observed coupling per band as the coupling and the standard deviation across the band as the error in that figure.

It is also agreed that the large scatter observed on e.g. the HEB bands can not be related to optical coupling issues. This is probably more related to the calibration measurement itself, including stability and standing wave issues. However, the average plateau-like structure in the HBB coupling plots (band dependent average) might actually be quite real mimicking a combined optical coupling / emissivity / temperature effect varying from band to band which we need to derive from our calibration data. It is considered perfectly plausible that these combined effects can be as large as a couple of percent, i.e. it is not excluded to detect coupling ratios of order 96-97% from the modelling point of view, although the statistical evidence is small at least in bands 2-4.

7.3 HRS data

A similar analysis was performed on the HRS, for which data have been taken in parallel. This data-set is used as a redundant measurement to check that no back-end related artefact could lead to different coupling numbers. We found that both back-ends end up giving fully compatible results. Figure 11 shows the fitted coupling found for each of the back-ends, with their error bars. The table below summarizes them in the same fashion as table 2.

For the source coupling calibration product, we decided to stick to the WBS data as they are supposed to sample a larger range of channels.

Band	Start Freq	Stop Freq	Coupling	Coup. Err.	Slope	Slope err.	Freq0
Cold couplings – HRS-H polarization							
1	494	620	0.991	1.8E-3	0	0	0
2	640	716	0.993	1.6E-3	0	0	0
3	816	942	0.996	1.2E-3	0	0	0
4	1060	1108	0.997	1.4E-3	0	0	0
5	1116	1266	0.987	1.7E-2	0	0	0
6	1432	1692	0.991	5.7E-2	0	0	0
7	1708	1908	0.996	5.3E-2	0	0	0
Hot couplings – HRS-H polarization							
1	498	624	0.965	8.6E-4	1.67E-4	1.96E-5	561
2	640	716	0.987	4.3E-3	0	0	0
3	808	938	0.989	2.5E-3	0	0	0
4	1064	1112	0.996	2.2E-3	0	0	0
5	1116	1258	0.993	1.8E-2	0	0	0
6	1432	1692	0.976	4.1E-2	0	0	0
7	1704	1908	0.969	6.7E-2	0	0	0
Cold couplings – HRS-V polarization							
1	494	620	0.991	1.6E-3	0	0	0
2	640	716	0.988	9.8E-3	0	0	0
3	816	942	0.993	1.8E-3	0	0	0
4	1060	1108	0.994	3.0E-3	0	0	0
5	1116	1266	0.990	1.3E-2	0	0	0
6	1432	1692	0.988	5.4E-2	0	0	0
7	1708	1908	1.004	6.2E-2	0	0	0
Hot couplings – HRS-V polarization							
1	498	624	0.971	1.4E-3	4.84E-5	3.25E-5	561
2	640	716	0.990	1.2E-2	0	0	0
3	808	938	0.987	5.4E-3	0	0	0
4	1064	1112	0.998	3.9E-3	0	0	0
5	1116	1258	0.999	1.2E-2	0	0	0
6	1432	1692	0.976	7.6E-2	0	0	0
7	1704	1908	0.972	9.9E-2	0	0	0

Table 3: Final coupling numbers for each mixer as derived from the HRS

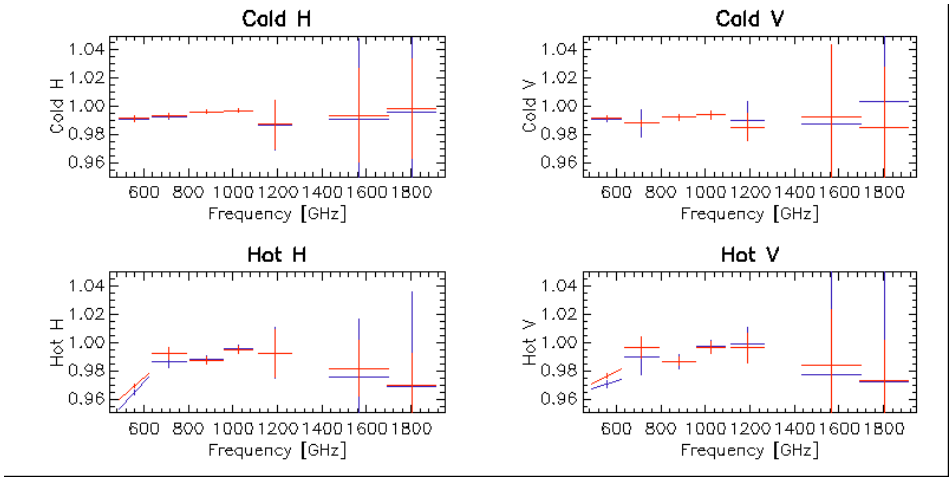

Fig 11: Comparative results from the WBS (red) and the HRS (blue)

7.4 Source coupling plots

The following figures illustrate the data used in the fitting process, as well as the fit results. For all mixer bands, we show all available measurements from the February, April and June campaign. Red diamond symbols indicate the data used for the fit, which were filtered from the global data-set based on a case-by-case inspection of the base-line quality (excess noise, standing wave, etc). The February and April data-set points are indicated with black crosses, while June data are shown as blue crosses. Plots are shown for each individual bands, as well as for the full data-set.

Figures 26 and 27 (resp. 46 and 47 for the HRS) show the overall distribution of the coupling for the full HIFI range. The numbers used in the WBS plots are tabulated in the following excel attachments:

Y:\fm_ilt_4\radiometry\report\HI

Y:\fm_ilt_4\radiometry\report\HI

Finally Figures 28 to 31 show the full WBS spectral data-set used in this analysis, illustrating the detailed shapes of the spectra depending on the LO sub-band, and showing clearly some of the effects described in this report.

7.5 Archival data

The numbers in the table above will be stored as calibration products in a dedicated pool. Similarly, the full couplings data-set and the corresponding spectra will be kept in simple

pools, allowing future re-processing, if necessary, without having to access any data-base, or run the full pipeline.

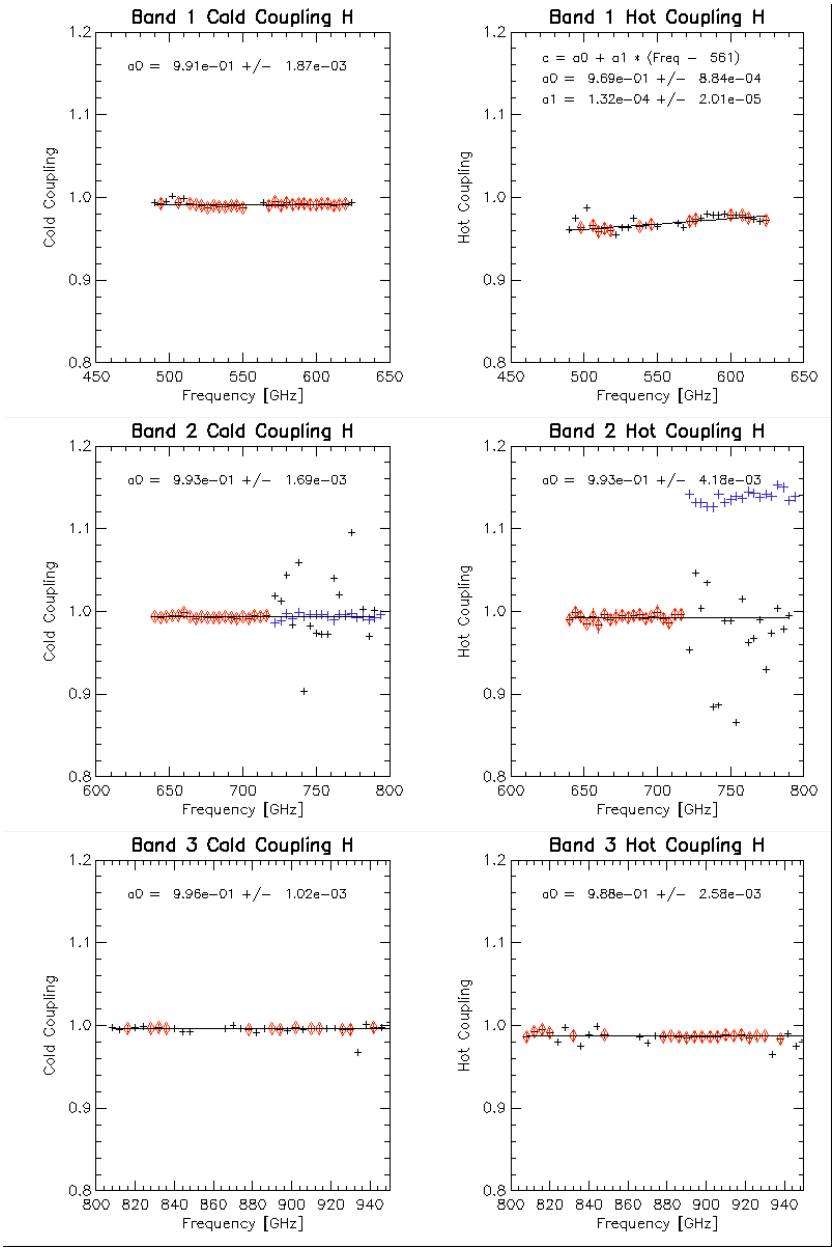
Band 1 Cold Coupling H
a0 = 9.91e-01 +/- 1.87e-03
Cold Coupling
Frequency [GHz]
Band 1 Hot Coupling H
c = a0 + a1 * (Freq - 561)
a0 = 9.69e-01 +/- 8.84e-04
a1 = 1.32e-04 +/- 2.01e-05
Hot Coupling
Frequency [GHz]
Band 2 Cold Coupling H
a0 = 9.93e-01 +/- 1.69e-03
Cold Coupling
Frequency [GHz]
Band 2 Hot Coupling H
a0 = 9.93e-01 +/- 4.18e-03
Hot Coupling
Frequency [GHz]
Band 3 Cold Coupling H
a0 = 9.96e-01 +/- 1.02e-03
Cold Coupling
Frequency [GHz]
Band 3 Hot Coupling H
a0 = 9.88e-01 +/- 2.58e-03
Hot Coupling
Frequency [GHz]

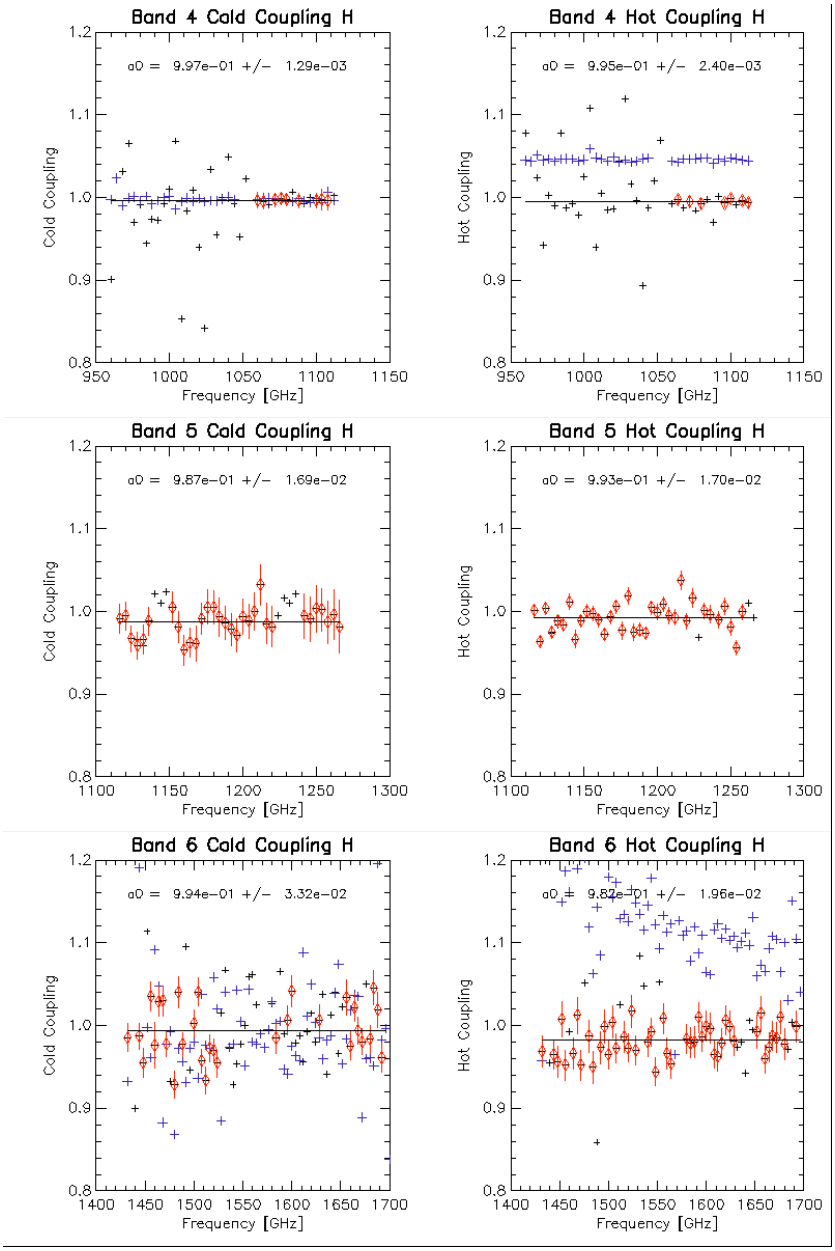
Band 4 Cold Coupling H
a0 = 9.97e-01 +/- 1.29e-03
Cold Coupling
Frequency [GHz]
Band 4 Hot Coupling H
a0 = 9.95e-01 +/- 2.40e-03
Hot Coupling
Frequency [GHz]
Band 5 Cold Coupling H
a0 = 9.87e-01 +/- 1.69e-02
Cold Coupling
Frequency [GHz]
Band 5 Hot Coupling H
a0 = 9.93e-01 +/- 1.70e-02
Hot Coupling
Frequency [GHz]
Band 6 Cold Coupling H
a0 = 9.94e-01 +/- 3.32e-02
Cold Coupling
Frequency [GHz]
Band 6 Hot Coupling H
a0 = 9.82e-01 +/- 1.96e-02
Hot Coupling
Frequency [GHz]

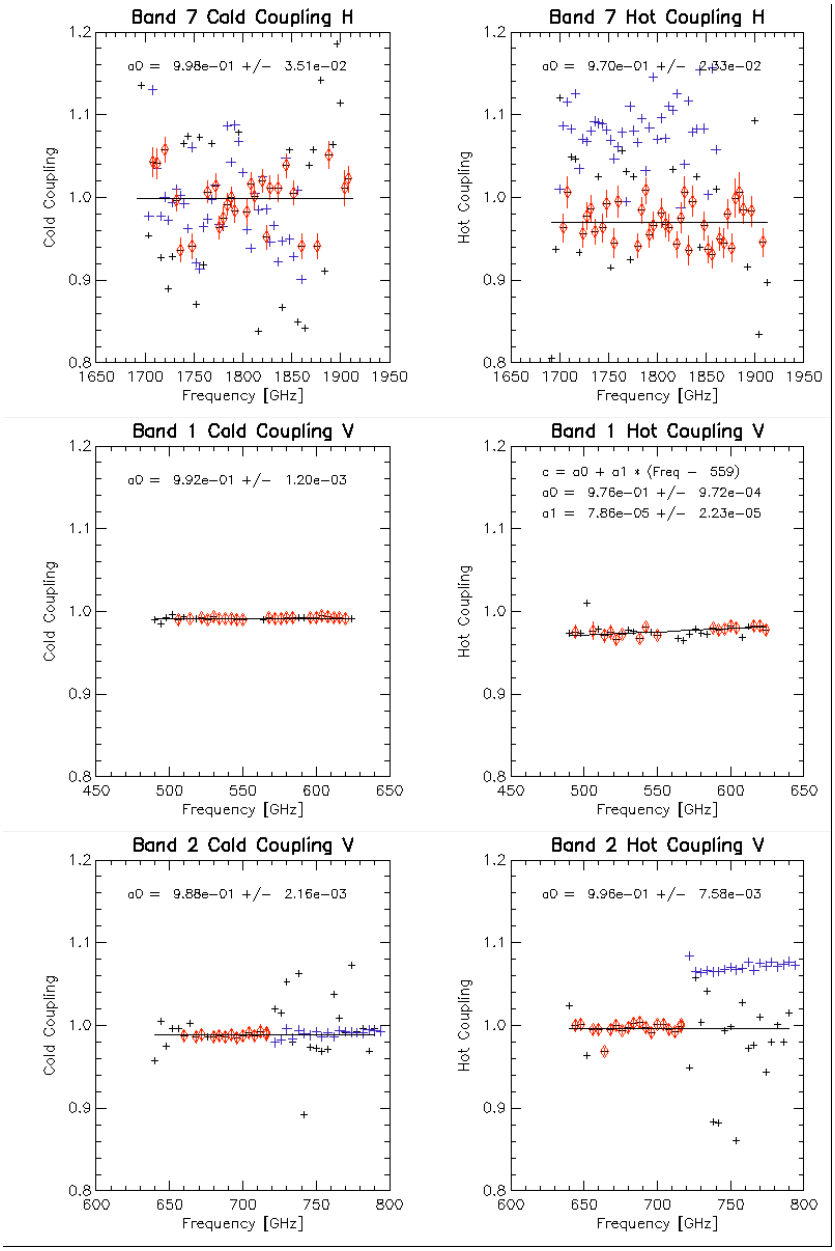
Band 7 Cold Coupling H
a0 = 9.98e-01 +/- 3.51e-02
Cold Coupling
Frequency [GHz]
Band 7 Hot Coupling H
a0 = 9.70e-01 +/- 2.33e-02
Hot Coupling
Frequency [GHz]
Band 1 Cold Coupling V
a0 = 9.92e-01 +/- 1.20e-03
Cold Coupling
Frequency [GHz]
Band 1 Hot Coupling V
c = a0 + a1 * (Freq - 559)
a0 = 9.76e-01 +/- 9.72e-04
a1 = 7.86e-05 +/- 2.23e-05
Hot Coupling
Frequency [GHz]
Band 2 Cold Coupling V
a0 = 9.88e-01 +/- 2.16e-03
Cold Coupling
Frequency [GHz]
Band 2 Hot Coupling V
a0 = 9.96e-01 +/- 7.58e-03
Hot Coupling
Frequency [GHz]

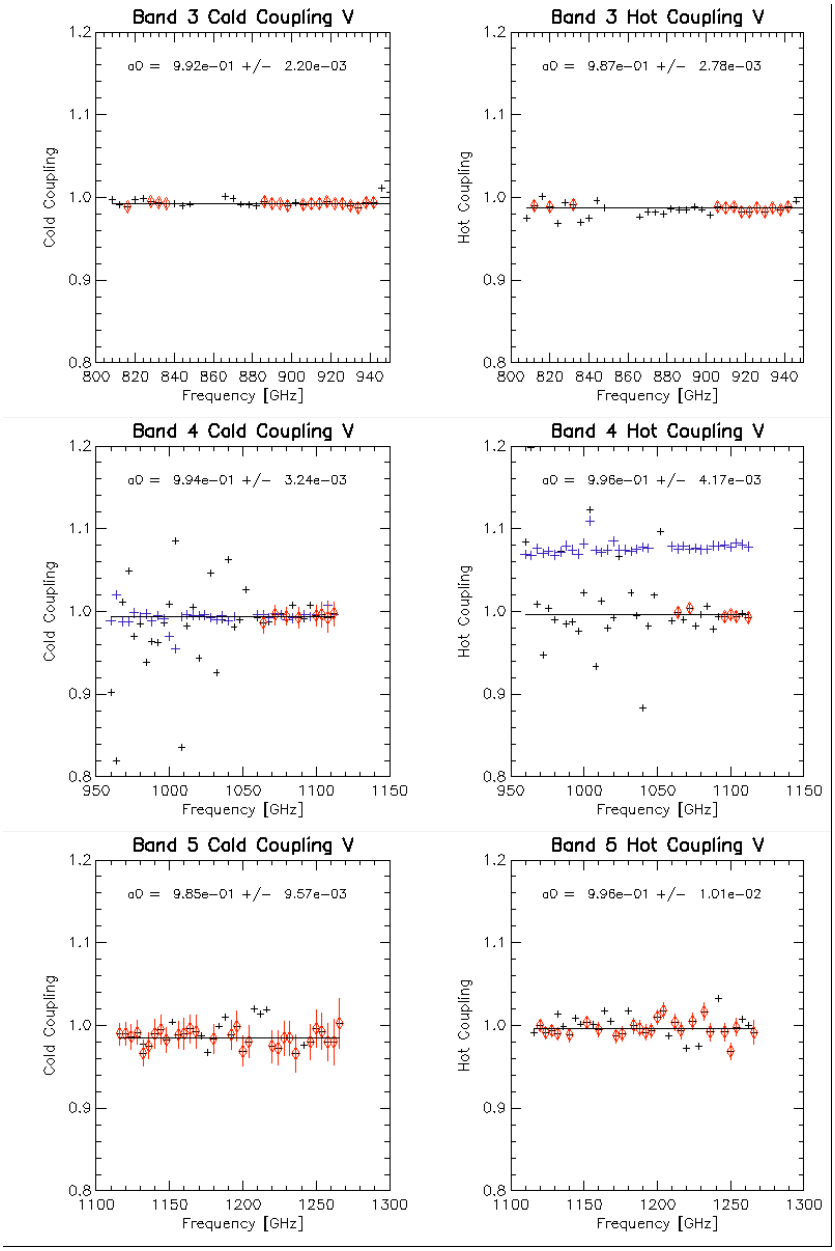
Band 3 Cold Coupling V
a0 = 9.92e-01 +/- 2.20e-03
Cold Coupling
Frequency [GHz]
Band 3 Hot Coupling V
a0 = 9.87e-01 +/- 2.78e-03
Hot Coupling
Frequency [GHz]
Band 4 Cold Coupling V
a0 = 9.94e-01 +/- 3.24e-03
Cold Coupling
Frequency [GHz]
Band 4 Hot Coupling V
a0 = 9.96e-01 +/- 4.17e-03
Hot Coupling
Frequency [GHz]
Band 5 Cold Coupling V
a0 = 9.85e-01 +/- 9.57e-03
Cold Coupling
Frequency [GHz]
Band 5 Hot Coupling V
a0 = 9.96e-01 +/- 1.01e-02
Hot Coupling
Frequency [GHz]

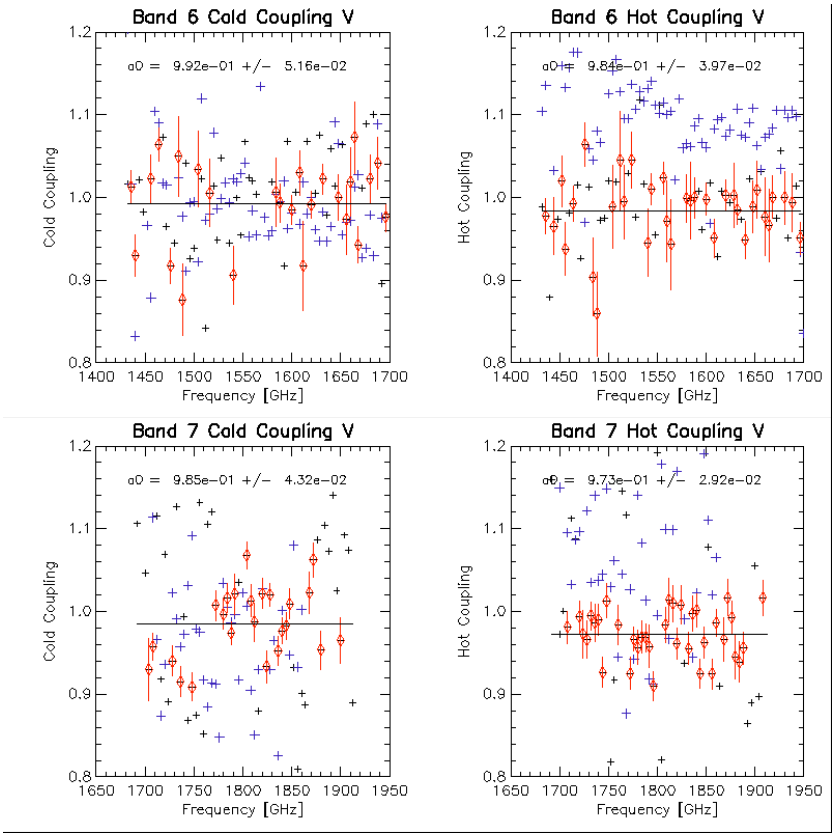

Fig. 12 to 25: data-set used to measure the source coupling, and associated fits for the WBS data. See text for details

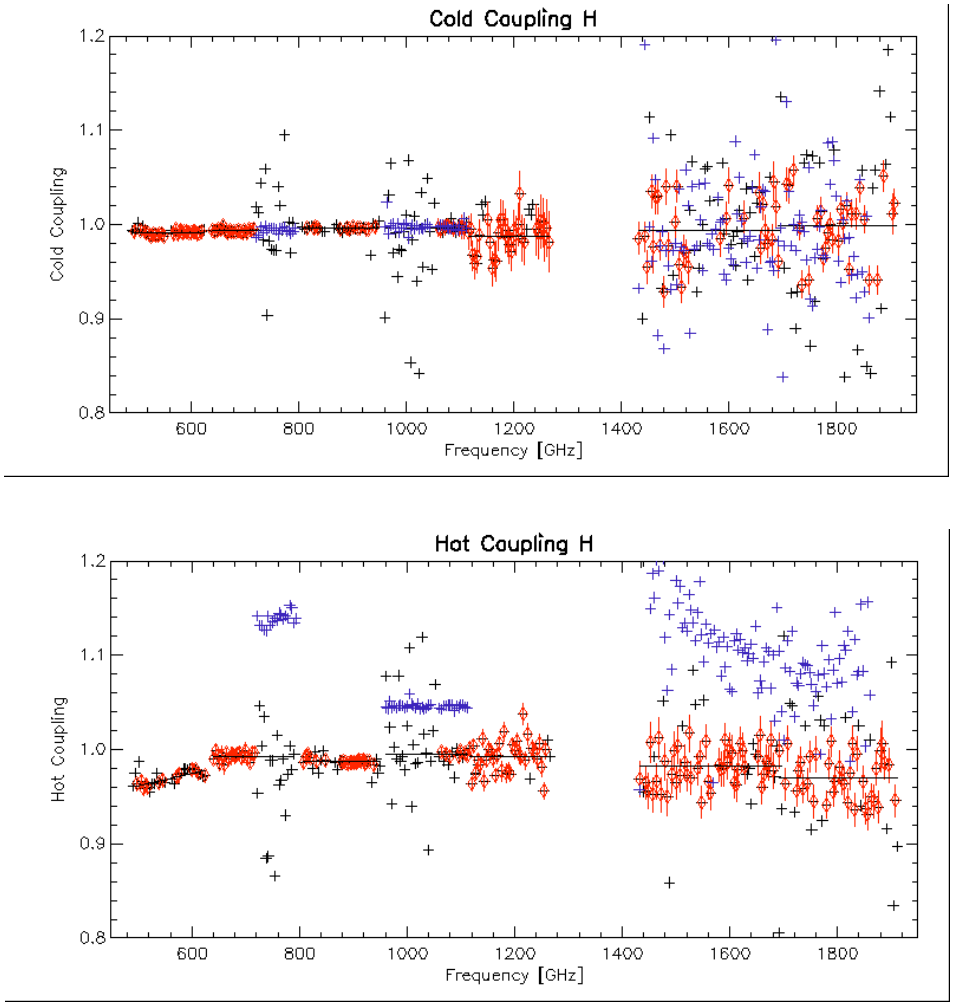

Fig. 26: Compilation of all data for the H-polarization as derived from the WBS

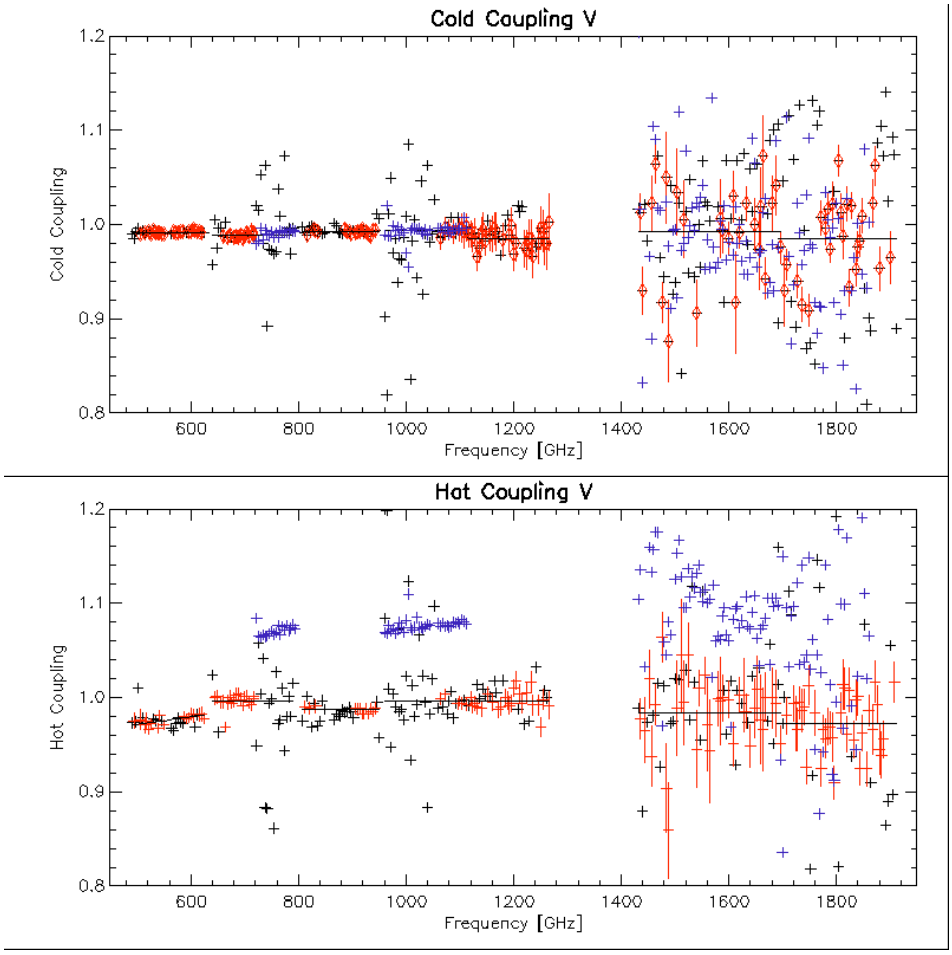

Fig. 27: Compilation of all data for the V-polarization as derived from the WBS

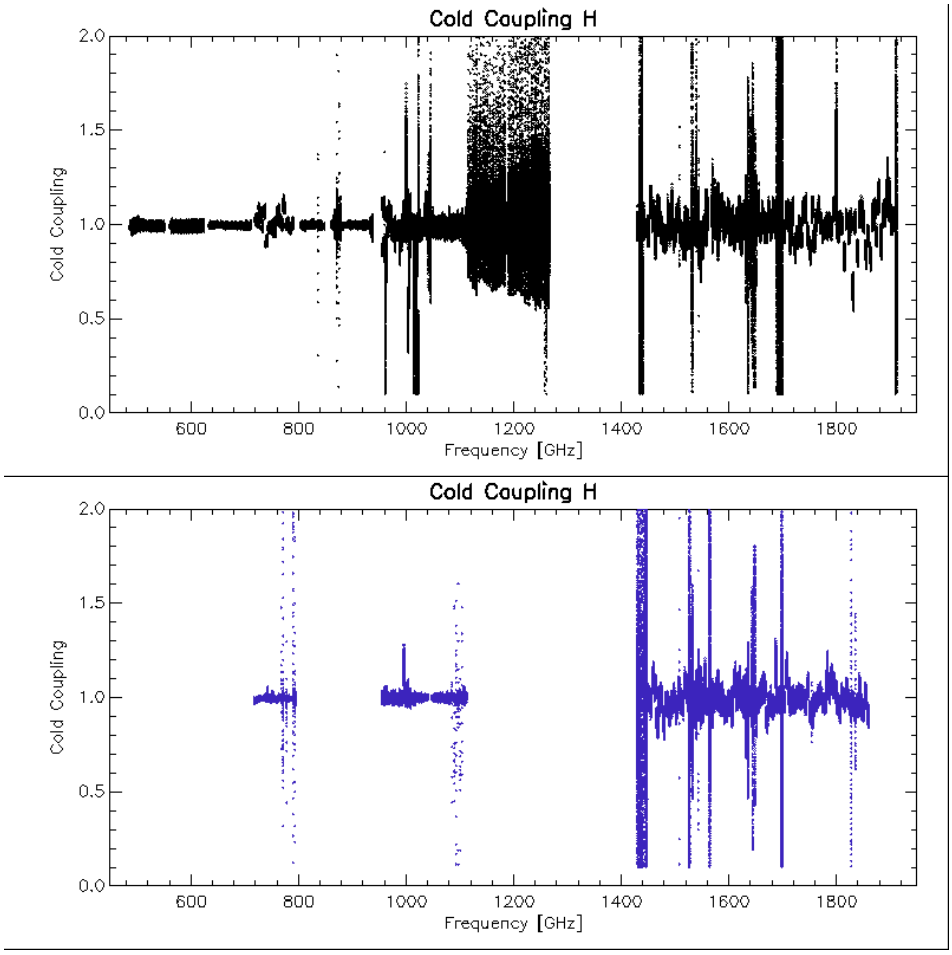

Fig. 28: Full channel cold coupling spectra for the February + April and the June data-set respectively. Data are for the H-polarization as derived from the WBS

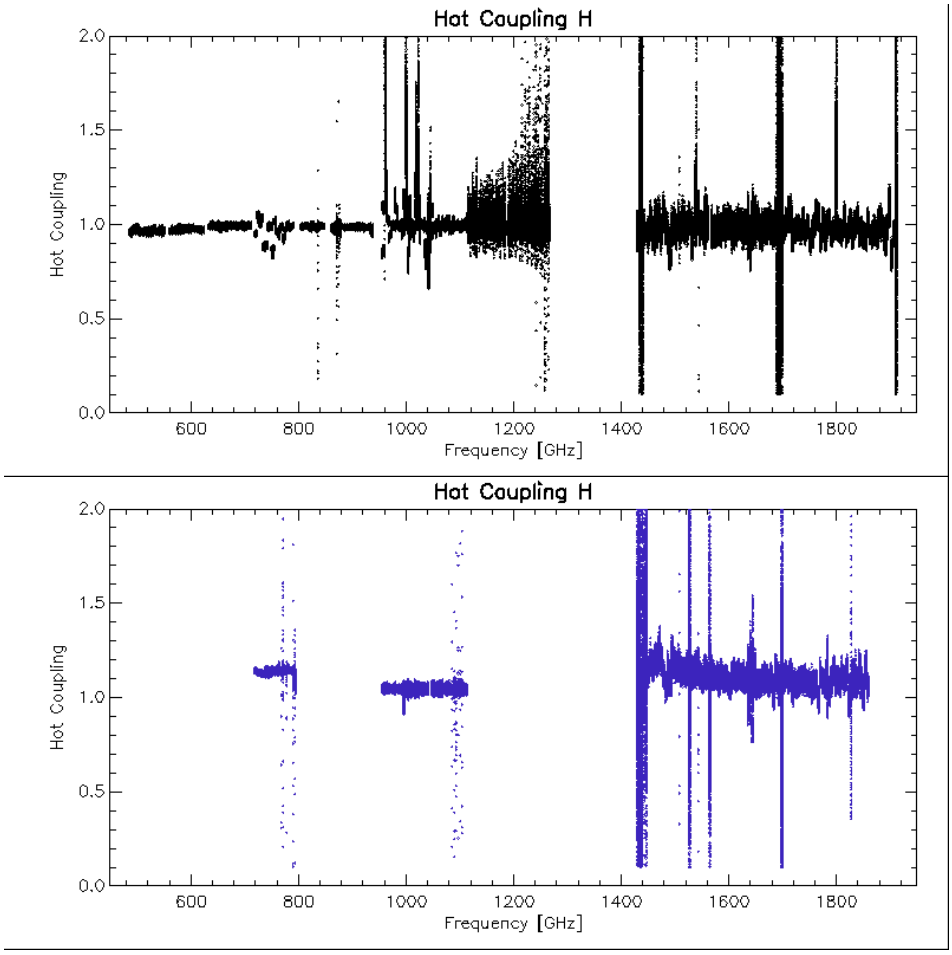

Fig. 29: Full channel hot coupling spectra for the February + April and the June data-set respectively. Data are for the H-polarization as derived from the WBS

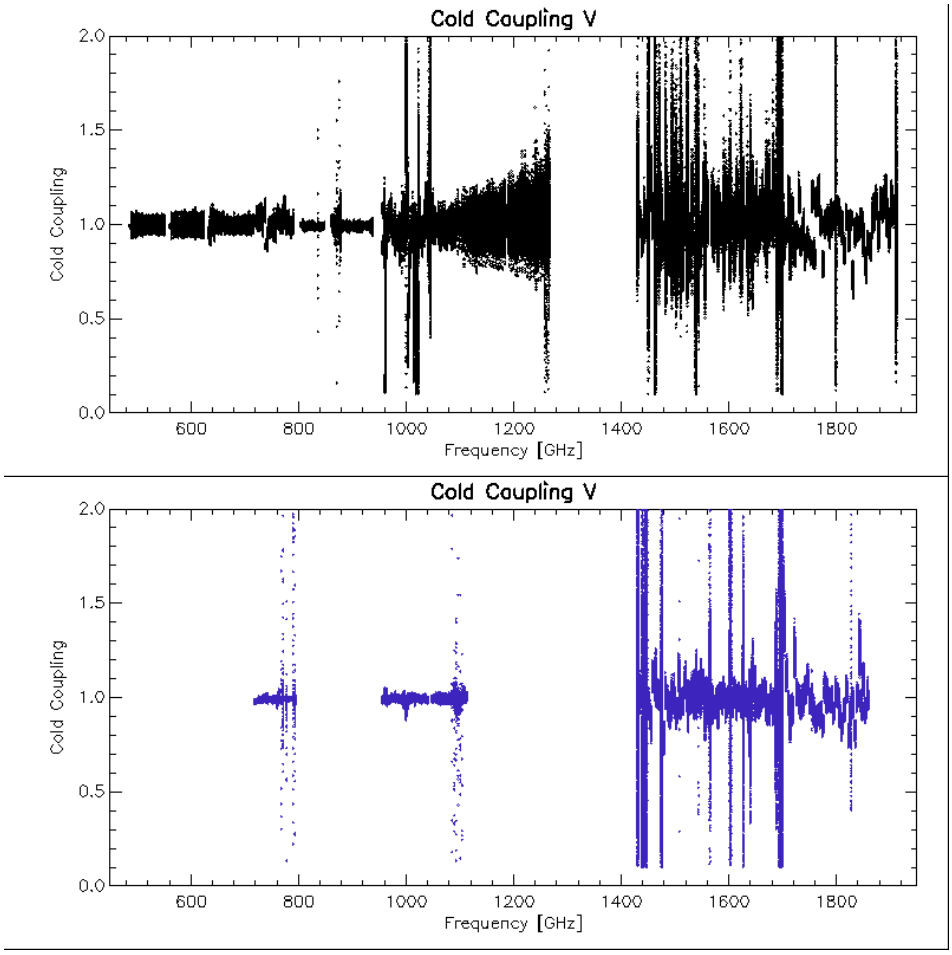

Fig. 30: Full channel cold coupling spectra for the February + April and the June data-set respectively. Data are for the V-polarization as derived from the WBS

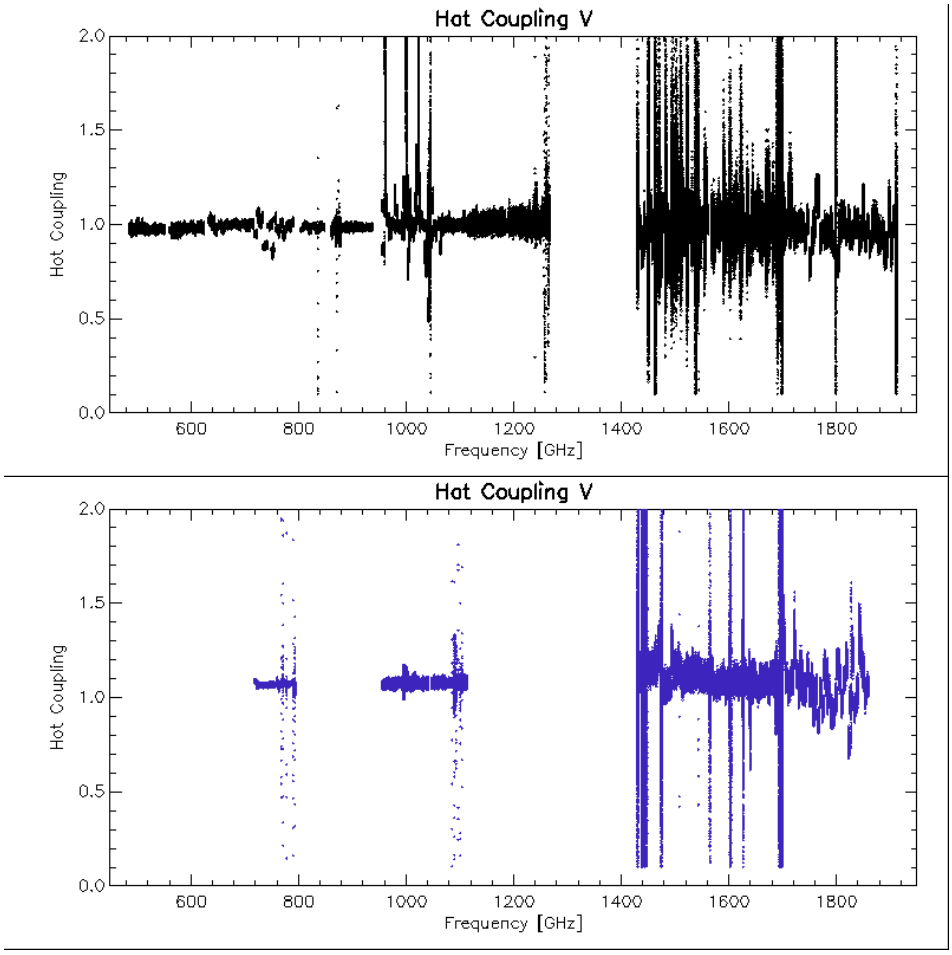

Fig. 31: Full channel hot coupling spectra for the February + April and the June data-set respectively. Data are for the V-polarization as derived from the WBS

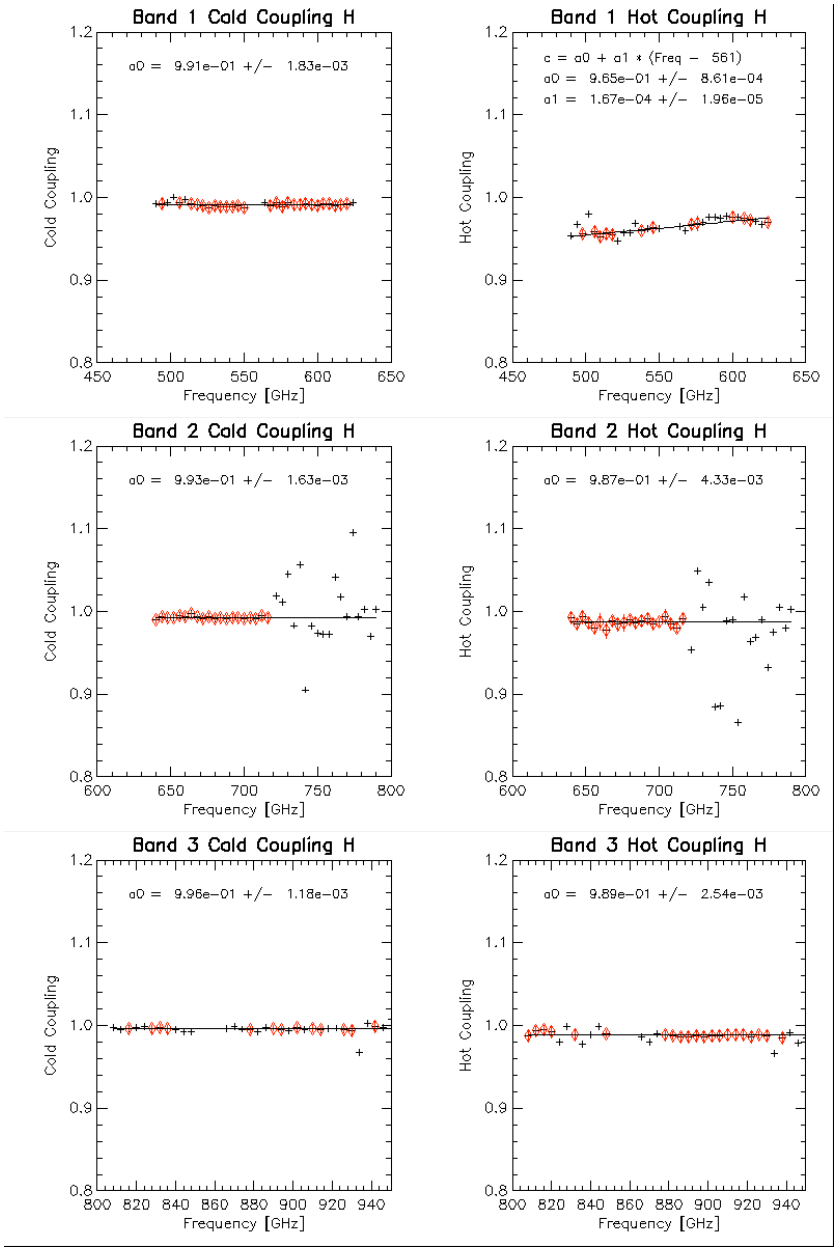
Band 1 Cold Coupling H
a0 = 9.91e-01 +/- 1.83e-03
Cold Coupling
Frequency [GHz]
Band 1 Hot Coupling H
c = a0 + a1 * (Freq - 561)
a0 = 9.65e-01 +/- 8.61e-04
a1 = 1.67e-04 +/- 1.96e-05
Hot Coupling
Frequency [GHz]
Band 2 Cold Coupling H
a0 = 9.93e-01 +/- 1.63e-03
Cold Coupling
Frequency [GHz]
Band 2 Hot Coupling H
a0 = 9.87e-01 +/- 4.33e-03
Hot Coupling
Frequency [GHz]
Band 3 Cold Coupling H
a0 = 9.96e-01 +/- 1.18e-03
Cold Coupling
Frequency [GHz]
Band 3 Hot Coupling H
a0 = 9.89e-01 +/- 2.54e-03
Hot Coupling
Frequency [GHz]

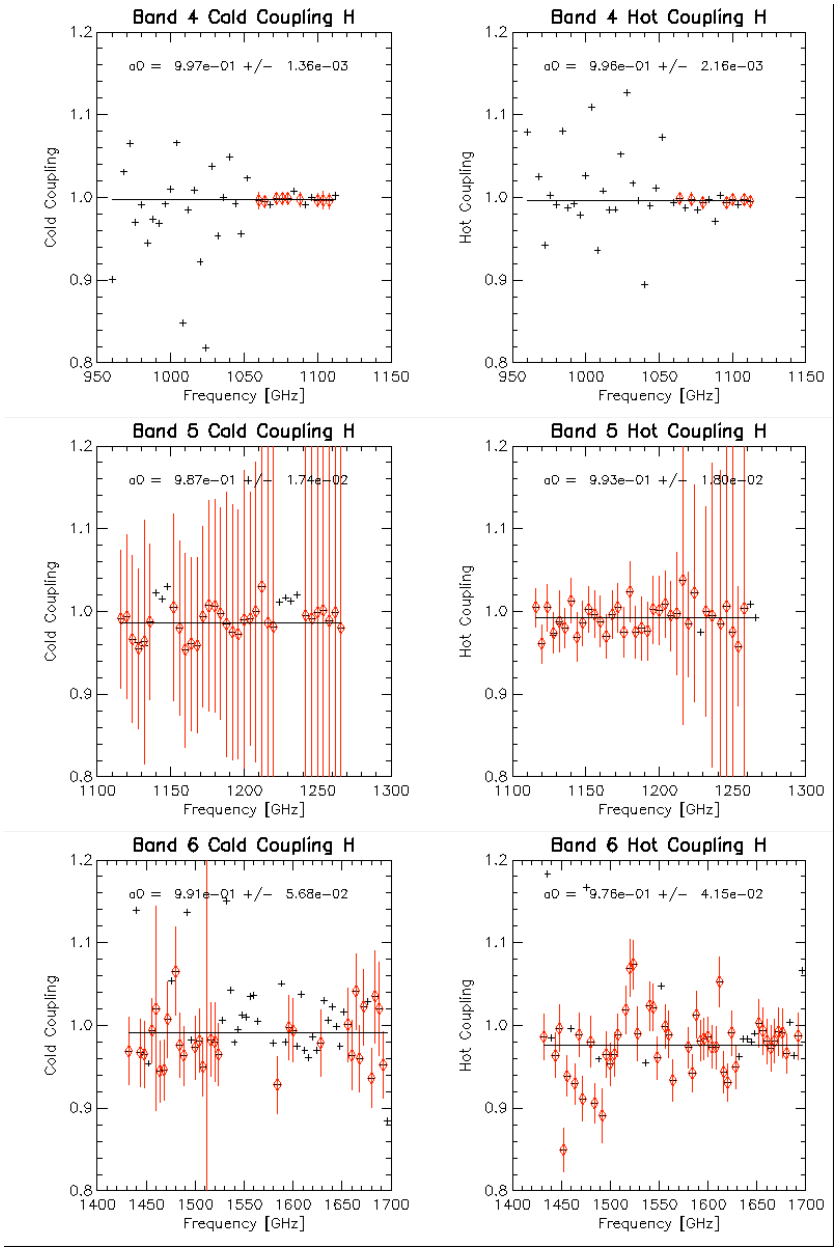
Band 4 Cold Coupling H
a0 = 9.97e-01 +/- 1.36e-03
Band 4 Hot Coupling H
a0 = 9.96e-01 +/- 2.16e-03
Band 5 Cold Coupling H
a0 = 9.87e-01 +/- 1.74e-02
Band 5 Hot Coupling H
a0 = 9.93e-01 +/- 1.80e-02
Band 6 Cold Coupling H
a0 = 9.91e-01 +/- 5.68e-02
Band 6 Hot Coupling H
a0 = 9.76e-01 +/- 4.15e-02
Cold Coupling
Hot Coupling
Frequency [GHz]

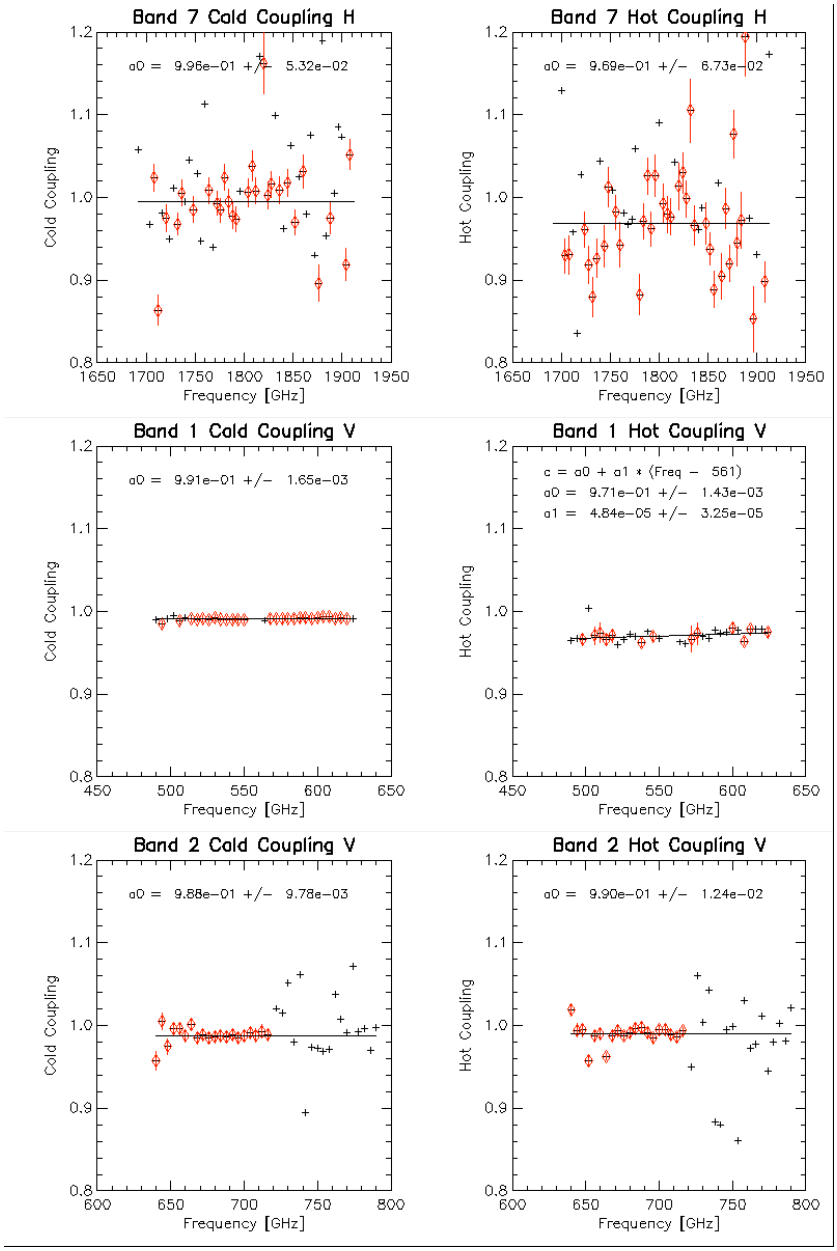
Band 7 Cold Coupling H
a0 = 9.96e-01 +/- 5.32e-02
Cold Coupling
Frequency [GHz]
Band 7 Hot Coupling H
a0 = 9.69e-01 +/- 6.73e-02
Hot Coupling
Frequency [GHz]
Band 1 Cold Coupling V
a0 = 9.91e-01 +/- 1.65e-03
Cold Coupling
Frequency [GHz]
Band 1 Hot Coupling V
c = a0 + a1 * (Freq - 561)
a0 = 9.71e-01 +/- 1.43e-03
a1 = 4.84e-05 +/- 3.25e-05
Hot Coupling
Frequency [GHz]
Band 2 Cold Coupling V
a0 = 9.88e-01 +/- 9.78e-03
Cold Coupling
Frequency [GHz]
Band 2 Hot Coupling V
a0 = 9.90e-01 +/- 1.24e-02
Hot Coupling
Frequency [GHz]

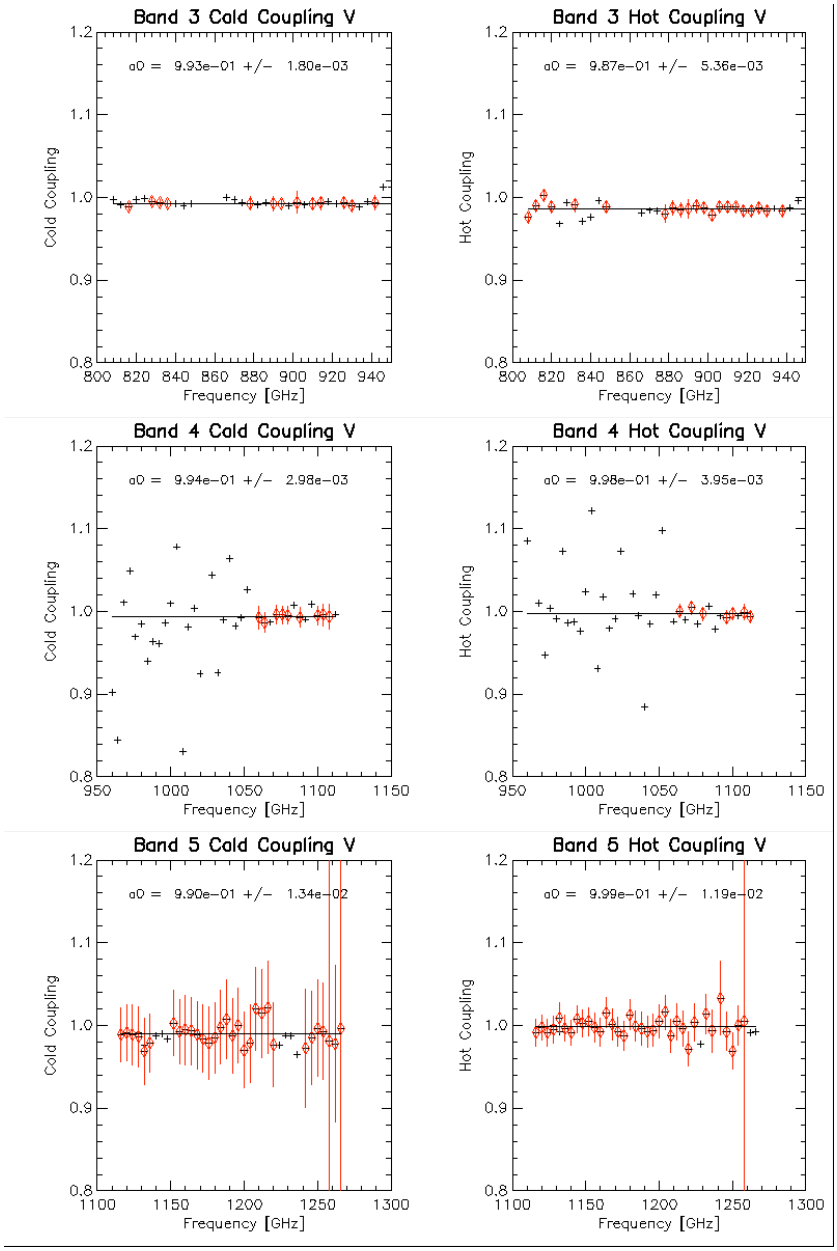
Band 3 Cold Coupling V
a0 = 9.93e-01 +/- 1.80e-03
Band 3 Hot Coupling V
a0 = 9.87e-01 +/- 5.36e-03
Band 4 Cold Coupling V
a0 = 9.94e-01 +/- 2.98e-03
Band 4 Hot Coupling V
a0 = 9.98e-01 +/- 3.95e-03
Band 5 Cold Coupling V
a0 = 9.90e-01 +/- 1.34e-02
Band 5 Hot Coupling V
a0 = 9.99e-01 +/- 1.19e-02
Cold Coupling
Hot Coupling
Frequency [GHz]

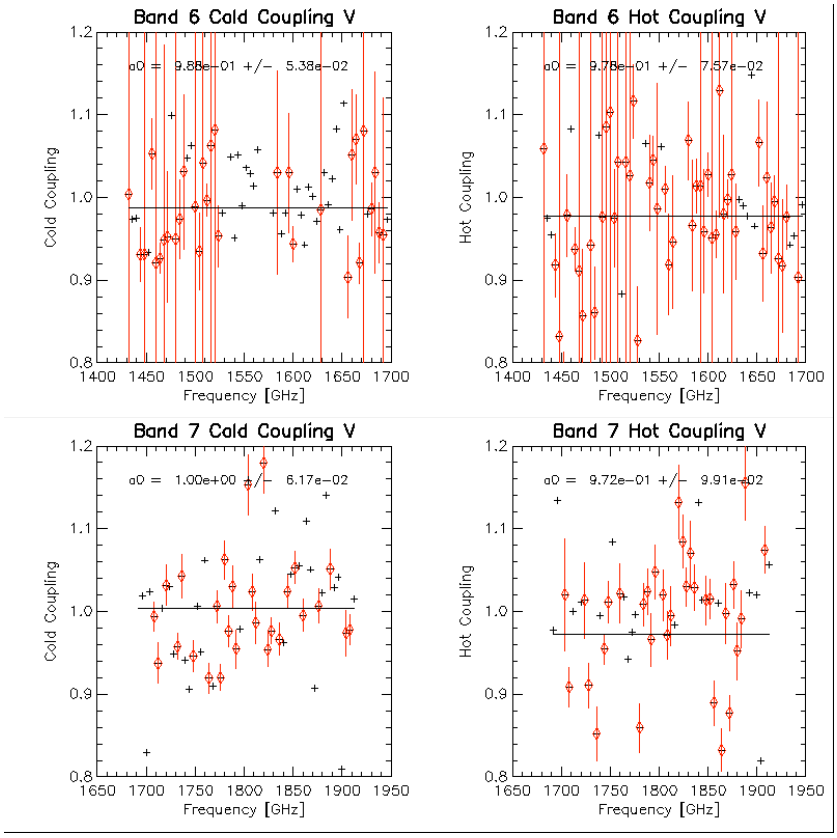

Fig. 32 to 45: data-set used to measure the source coupling, and associated fits for the HRS data. See text for details

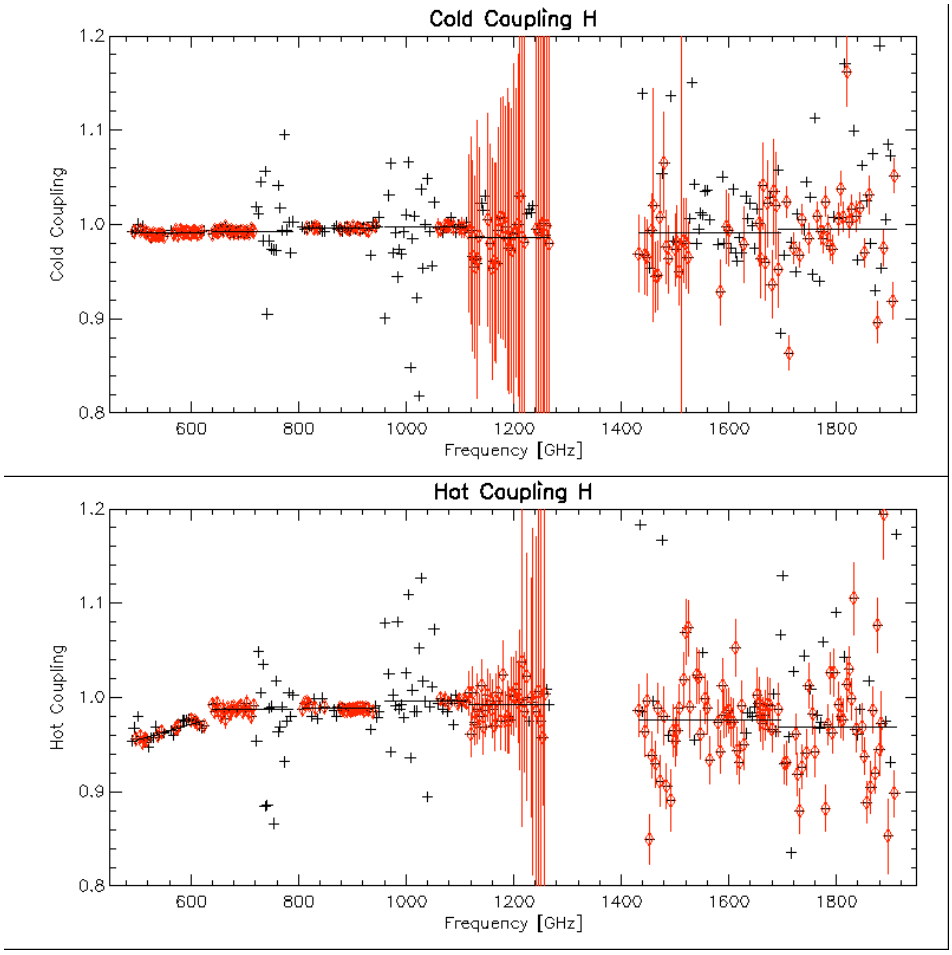

Fig. 46: Compilation of all data for the H-polarization as derived from the HRS

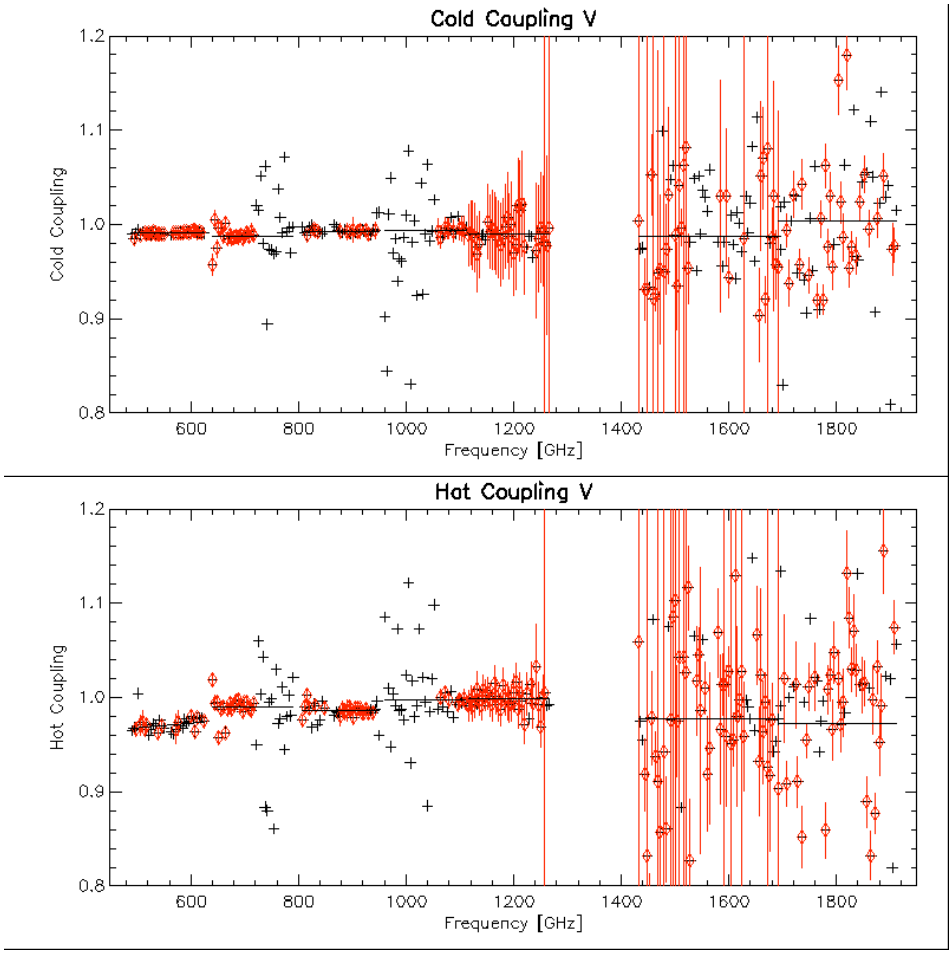

Fig. 47: Compilation of all data for the V-polarization as derived from the HRS